Multivalent BARD1-nucleosome interactions facilitate H2A ubiquitylation by BRCA1/BARD1

Samuel R. Witus[1], Lisa M. Tuttle[1], Alex Zelter[1], Klaiten E. Kermoade[1], Damien B. Wilburn[2,3], Weixing Zhao[4], Trisha N. Davis[1], Peter S. Brzovic[1], Rachel E. Klevit[1,*]

1. Department of Biochemistry, University of Washington, Seattle, WA.
2. Department of Genome Sciences, University of Washington, Seattle, WA.
3. Department of Chemistry and Biochemistry, The Ohio State University, Columbus, OH.
4. University of Texas Health Science Center at San Antonio, Department of Biochemistry and Structural Biology. San Antonio, TX.

* Corresponding author email: klevit@uw.edu

Abstract

BRCA1/BARD1 is a tumor suppressor E3 ubiquitin (Ub) ligase complex with roles in DNA damage repair and in transcriptional regulation. The N-terminal RING domains of BRCA1/BARD1 interact with nucleosomes to facilitate mono-ubiquitylation of distinct lysine residues on the extreme C-terminal tail of histone H2A. These enzymatic domains constitute only a small fraction of the total sequence of the heterodimer, raising the possibility of functional interactions with chromatin that are mediated through other parts of the protein. Possible interaction sites include the BARD1 C-terminal domains that bind to nucleosomes containing the DNA damage signal H2A K15-Ub and H4 K20me0, as well as portions of the expansive intrinsically disordered regions found in both subunits that have been reported to bind to DNA with unknown functional significance. Using full-length and truncated forms of BRCA1/BARD1 and a collection of designer chromatin substrates, we reveal novel interactions that support robust H2A ubiquitylation activity mediated through a high-affinity, intrinsically disordered DNA-binding region of BARD1. These interactions can be specifically inhibited by the presence of specialized DNA structures that represent intermediates during DNA damage and repair processes. We also identify distinct complexes between BRCA1/BARD1 and chromatin that depend on the presence of H2A K15-Ub, including a complex that spans adjacent nucleosome units. Together, our findings reveal an extensive network of multivalent BARD1-nucleosome interactions that serve as a platform for BRCA1/BARD1-associated functions on chromatin.

33 **Introduction**

34 Mutations in *BRCA1* and *BARD1* increase lifetime risk of developing breast and ovarian cancer.
35 BRCA1 and BARD1 form a large, obligate heterodimeric complex (BRCA1/BARD1) that has
36 distinct roles in DNA double-stranded break (DSB) repair by homologous recombination (HR),
37 transcriptional regulation, and several other nuclear processes (Densham & Morris, 2019;
38 Mullan et al., 2006; Tarsounas & Sung, 2020). These functions are mediated, at least in part,
39 through a direct association with chromatin. Upon DNA damage, BRCA1/BARD1 is recruited to
40 damaged chromatin where it segregates with DNA repair factors (Kolas Nadine K. et al., 2007;
41 Mattiroli et al., 2012; Scully et al., 1997; Sobhian Bijan et al., 2007). Cancer-predisposing
42 mutations that disrupt BRCA1/BARD1 functions on chromatin lead to DNA-damage
43 hypersensitivity and genomic instability(Alenezi et al., 2020; Gudmundsdottir & Ashworth, 2006;
44 Krais & Johnson, 2020). BRCA1/BARD1 also has distinct roles in both stimulation and
45 repression of transcription through as yet incompletely defined mechanisms (Mullan et al.,
46 2006). A full understanding of how BRCA1/BARD1 interfaces with chromatin, where it exerts its
47 major biological functions, is therefore critical.
48
49 Nucleosomes, the organizing unit of chromatin, directly interact with BRCA1/BARD1 through
50 multiple direct binding interfaces (Witus et al., 2022). The N-terminal RING domains of BRCA1
51 and BARD1 form a heterodimer that constitute a RING-type E3 ubiquitin (Ub) ligase and provide
52 the only known enzymatic activity of BRCA1/BARD1 (Brzovic et al., 2001; Lorick et al., 1999;
53 Witus, Stewart, et al., 2021). The RING heterodimer binds to the histone surface of one pseudo-
54 symmetrical ‘face’ of a nucleosome to facilitate site-specific transfer of mono-Ub to a cluster of
55 lysine residues on the extreme C-terminal tail of canonical histone H2A variants (K125, K127,
56 and K129; collectively referred to henceforth as K127) (Hu et al., 2021; Kalb et al., 2014; Witus,
57 Burrell, et al., 2021). H2A lysine specificity is largely determined by the RING domain of BARD1.
58 This domain binds to a unique histone surface compared to structurally similar Ub ligase

complexes that target other lysine residues on H2A (e.g., K119 by RING1B/BMI1) (McGinty et al., 2014). The H2A ubiquitylation ("H2A-Ub") activity of BRCA1/BARD1 is thought to contribute to its function in DNA damage repair via HR by promoting long-range resection of broken DNA ends (Densham et al., 2016; Uckelmann et al., 2018). BRCA1/BARD1-dependent H2A-Ub activity is also implicated in the transcriptional repression of certain estrogen-metabolizing cytochrome P450 genes and the constitutive repression of α-satellite DNA regions (Stewart et al., 2018; Q. Zhu et al., 2011, 2018).

The BARD1 C-terminal domains (CTDs; **Figure 1A**) also bind to nucleosomes to facilitate DNA DSB repair via HR (Becker et al., 2021; Dai et al., 2021; Hu et al., 2021; Krais et al., 2021; Nakamura et al., 2019). The BARD1 CTDs specifically recognize nucleosomes that contain H2A K15-Ub (the product of the Ub ligase RNF168) and unmethylated H4 K20 (H4K20me0). Together, these signals serve as a binding platform for the recognition of damaged chromatin in S/G2 phases when a sister chromatid is available to template high-fidelity DNA repair via HR. The BARD1 CTDs and N-terminal BRCA1/BARD1 RING domains bind to a fully overlapping histone surface, precluding their simultaneous binding to one nucleosome face. Despite this, mono-nucleosomes with ubiquitin pre-installed at H2A K15 are better substrates for BRCA1/BARD1-dependent ubiquitylation of H2A K127 *in vitro* (Hu et al., 2021). This observation implies that both domains may bind to the same nucleosome unit, with each occupying one face. However, a cellular mechanism for histone modification crosstalk between H2A K15-Ub marks deposited by RNF168 and H2A K127-Ub marks deposited by BRCA1/BARD1 has yet to be established. Additionally, regions throughout the expansive intrinsically disordered segments of both BRCA1 and BARD1 are reported to bind to DNA, but the functional significance of such interactions in chromatin binding and H2A-Ub activity remains to be determined (Mark et al., 2005; Masuda et al., 2016; Simons et al., 2006; Zhao et al., 2017).

85

86 Although a minimal RING/RING heterodimer is sufficient to direct the transfer of mono-Ub to
87 H2A K127 in nucleosomes, full-length BRCA1/BARD1 heterodimers form stronger complexes
88 with unmodified nucleosome substrates and exhibit increased H2A-Ub activity (Hu et al., 2021;
89 Witus, Burrell, et al., 2021). This suggests that additional interactions between full-length
90 BRCA1/BARD1 and nucleosomes can occur in the absence of the DNA-damage specific H2A
91 K15-Ub histone marks. Because BRCA1/BARD1 performs diverse biological functions in the
92 nucleus including but not limited to DNA repair via HR, transcriptional regulation, stalled
93 replication fork protection, centrosome regulation, R-loop resolution, and cell-cycle regulation, it
94 is likely that the complex can be recruited to chromatin via signals not limited to H2A K15-Ub. In
95 pursuit of a wholistic understanding of BRCA1/BARD1 recruitment to chromatin, we sought to
96 characterize interactions with nucleosomes that lead to enhanced chromatin binding and H2A-
97 Ub activity in both the absence and presence of H2A K15-Ub marks.

98

99 Here, we identify an intrinsically disordered region of BARD1 adjacent to its RING domain that
100 strongly binds to both nucleosomal and extra-nucleosomal DNA, dramatically enhancing the
101 affinity of the complex and its H2A-Ub activity. The interactions can be modulated by specialized
102 DNA structures that are derived from the DNA damage repair process and can compete directly
103 with BARD1 binding to nucleosomal DNA. We incorporate our findings into a molecular
104 mechanism of recognition. Additionally, we provide evidence for multiple, distinct higher-order
105 chromatin complexes that contain H2A K15-Ub nucleosomes. These include the presence of
106 both a ‘wrapped’ complex with the BRCA1/BARD1 RING domains and BARD1 CTDs bound to
107 opposite sides of one nucleosome unit, as well a complex where these domains bind to
108 adjacent nucleosome units. Throughout, we evaluate the contribution of BARD1 DNA binding to
109 nucleosome affinity and H2A-Ub activity. Together, our findings reveal an extensive network of

110 multivalent BARD1-nucleosome interactions that serve as a platform for BRCA1/BARD1-
111 associated functions on chromatin.
112
113 **Results**
114 **Identification of a BARD1 region that supports increased H2A ubiquitylation activity**
115 BRCA1/BARD1 is a large, obligate heterodimeric complex with distinct functional domains and
116 long intrinsically disordered regions (IDRs**; Figure 1A)**. A minimal complex composed of the two
117 N-terminal RINGs of BRCA1 (1-110) and BARD1 (26-140; $BRCA1^{RING}$/$BARD1^{RING}$) is sufficient
118 to direct site-specific mono-ubiquitylation of nucleosomal histone H2A at K127 (Kalb et al.,
119 2014). We and others previously reported that full-length BRCA1/BARD1 (~300 kDa) exhibits
120 faster H2A-Ub kinetics and stronger binding to mono-nucleosomes than the minimal
121 RING/RING complex (~25 kDa; **Figure 1—figure supplement 1A-C**) (Hu et al., 2021; Witus,
122 Burrell, et al., 2021). To uncover regions of BRCA1 or BARD1 responsible for increased H2A-
123 Ub activity and binding affinity, we generated a series of heterodimers with truncations in one or
124 the other subunit **(Figure 1—figure supplement 2 and Extended Data Table I)**.
125
126 To measure contributions from the BRCA1 subunit, heterodimers containing full-length BARD1
127 and three different BRCA1 constructs were compared: full-length BRCA1 ($BRCA1^{FL}$), a clinically
128 relevant allele missing ~1100 residues in the expansive IDR region ($BRCA1^{\Delta 11q}$), and the
129 minimal BRCA1 RING fragment **(**$BRCA1^{RING}$**)**. All three heterodimers that contained full-length
130 BARD1 exhibited faster H2A-Ub kinetics than the minimal $BRCA1^{RING}$/$BARD1^{RING}$ complex
131 **(Figure 1—figure supplement 1C)**. Complexes containing truncated BRCA1 ($BRCA1^{RING}$ and
132 $BRCA1^{\Delta 11q}$) exhibited faster H2A-Ub kinetics than the full-length heterodimer. In contrast,
133 $BARD1^{RING}$-heterodimers containing $BRCA1^{FL}$ or $BRCA1^{\Delta 11q}$ exhibited diminished H2A-Ub
134 activity compared to the full-length complex **(Figure 1—figure supplement 1D)**. Together these

135 observations suggest that there may be inhibitory elements or alternative interactions involving
136 regions of BRCA1 in the full-length complex. Overall, the data indicate that BARD1 is
137 predominantly responsible for the enhanced H2A-Ub activity that is observed in the full-length
138 BRCA1/BARD1 complex.
139
140 To identify regions of BARD1 that contribute to increased H2A-Ub activity, the H2A-Ub kinetics
141 and nucleosome binding affinity of BRCA1^{RING}-heterodimers containing BARD1 truncations
142 were compared. Notably, BRCA1^{RING}/BARD1^{FL} heterodimers bind nucleosomes with ~1000-fold
143 higher affinity than the minimal BRCA1^{RING}/BARD1^{RING} complex and had markedly higher H2A-
144 Ub activity **(Figure 1B, C)**. Removal of the BARD1 Ank-BRCT C-terminal domains (BARD1$^{\Delta CTD}$)
145 or truncation back to residue 216 in the putative intrinsically disordered region (BARD1^{216}) had
146 minimal impact on H2A-Ub activity and nucleosome binding **(Figure 1B, C)**. However,
147 truncation to BARD1 residue 193 (BARD1^{193}) caused a substantial decrease in H2A-Ub activity
148 and a ~10-fold reduction in binding affinity, implying a role for residues between 194 and 216.
149 Consistent with this, deletion of the first half of the BARD1 IDR (BARD1$^{\Delta 140-270}$) greatly
150 diminished H2A-Ub activity **(Figure 1—figure supplement 1E)**. A more targeted deletion
151 (BARD1$^{\Delta 194-216}$) only modestly decreased H2A-Ub activity, suggesting the presence of additional
152 or compensatory nucleosome interaction sites in BARD1. Although deletion of residues 140-270
153 decreased nucleosome binding affinity by ~3-fold relative to full-length BARD1, the affinity is still
154 considerably stronger than the minimal RING/RING heterodimer or BARD1^{193} truncations
155 **(Figure 1—figure supplement 1F)**. To assess intrinsic nucleosome-binding function of the
156 BARD1 IDR, constructs containing only either the N-terminal half (residues 124-270) or the C-
157 terminal half (residues 269-424) were analyzed. Each IDR-only construct exhibited nucleosome
158 binding by EMSA **(Figure 1—figure supplement 1G).** The apparent dispensability of BARD1
159 IDR residues past 216 in H2A-Ub activity may indicate a requirement for specific types of

160 interactions that our binding assay is not sensitive to **(Figure 1B)**. In total, a region within the
161 IDR of BARD1 (BARD1 194-216) was identified that is important for productive nucleosome
162 binding that supports increased H2A-Ub activity. Importantly, these data also demonstrate that
163 the BARD1 CTDs are dispensable for mono-nucleosome binding and for H2A-Ub activity on
164 nucleosomes that lack H2A K15-Ub marks.
165
166 **Additional BARD1-nucleosome interactions are mediated through DNA binding**
167 Having identified non-RING regions of BARD1 that contribute to increased H2A-Ub activity and
168 nucleosome binding, we sought to characterize the molecular interactions involved. BARD1
169 residues 141-216 are in a large internal segment predicted to be intrinsically disordered (124-
170 424) (McGuffin et al., 2000). To our knowledge, whether this region of BARD1 is fully disordered
171 has not been explicitly tested. Nuclear magnetic resonance (NMR) $^{1}H^{15}N$-HSQC spectra of ^{15}N-
172 labelled BARD1 fragments containing residues 124-270, 269-424, and 124-424 all exhibited
173 narrow ^{1}H chemical shift dispersion that is consistent with an IDR **(Figure 2—figure**
174 **supplement 1A, B)**. Furthermore, the spectra corresponding to the two halves (124-270 and
175 269-424) overlay well with the spectrum of the full region, indicating that the two halves behave
176 independently of one another **(Figure 2—figure supplement 1B)**.
177
178 The BARD1 region that enhances nucleosome binding and H2A-Ub activity identified above is
179 contained within the first half of the IDR, spanning residues 124-270. This region has been
180 reported to bind to double-stranded DNA and specialized DNA structures containing base-pair
181 mismatch (discussed below) (Zhao et al., 2017). The sequence of BARD1 124-270 is largely
182 conserved across orthologs and its amino acid content is strongly basic **(Figure 2—figure**
183 **supplement 1C)**. We hypothesized that observed contributions to H2A-Ub and nucleosome
184 binding activity from the disordered region outside the RING domain (BARD1 residues 141-216)
185 could be mediated through interactions with nucleosomal DNA. Several nucleosome-modifying

186 enzymes such as the methyltransferases DOT1L and COMPASS contain DNA-binding regions
187 adjacent to their catalytic domains that are required for full activity (Hsu et al., 2019; McGinty &
188 Tan, 2016, 2021; Worden et al., 2019, 2020). Indeed, we observed strong binding of BARD1
189 124-270 to nucleosomes and to free 147-bp '601' dsDNA by EMSA **(Figure 2—figure**
190 **supplement 2A)**.
191
192 For residue-level information, we performed NMR binding experiments with ^{15}N-labelled BARD1
193 124-270 and either a 36-bp dsDNA fragment or a 147-bp nucleosome **(Figure 2A and Figure**
194 **2—figure supplement 2B, respectively)**. Between these two titrants, only a full titration of the
195 dsDNA fragment was possible due to its smaller molecular weight than a nucleosome and
196 complex solubility considerations. The resulting spectral series identified a subset of resonances
197 that shift continuously as a function of DNA concentration **(Figure 2A**). A similar set of
198 resonances were perturbed (broadened in this case) upon addition of 147-bp nucleosome,
199 indicating that BARD1 employs similar residues to recognize nucleosomes and free dsDNA
200 **(Figure 2—figure supplement 2B)**. To overcome spectral overlap in the spectrum of BARD1
201 124-270, a smaller construct encompassing the putative DNA binding region identified in H2A-
202 Ub activity and nucleosome binding assays (BARD1 141-216, where residue 141 is the first to
203 extend beyond BARD1^{RING}) was assigned. Assignments from the smaller construct could be
204 transferred to the longer segment, enabling binding analysis by NMR in both contexts **(Figure**
205 **2A, B and Figure 2—figure supplement 2B, C)**. Secondary structure propensity (SSP)
206 predicted from the resonance assignments are consistent with the region being primarily
207 disordered, with helical propensity predicted for residues 191-201 and a weaker prediction of
208 extended structure towards the beginning of the construct **(Figure 2—figure supplement 3A).**
209
210 The largest backbone amide chemical shift perturbations (CSPs) due to dsDNA addition are
211 clustered in BARD1 residues 194-216, with smaller perturbations observed for residues 146-161

212 **(Figure 2B).** As well, ^{15}N dynamics measurements reveal that residues 146-161 undergo
213 changes in dynamics in the presence of dsDNA **(Figure 2—figure supplement 3B)**. Predicted
214 secondary structure from chemical shifts of BARD1 in the presence of 1 molar equivalent of
215 dsDNA indicate reduced helical propensity in residues 191-199 upon DNA binding **(Figure 2—**
216 **figure supplement 3A)**. Importantly, residues between 162-191 of BARD1 were relatively
217 unaffected by addition of dsDNA, consistent with the existence of specific DNA-binding regions.
218 Due to solubility and concentration limitations, we were unable to perform similar analysis on
219 nucleosome-bound samples. Nevertheless, the similar $^{1}H^{15}N$-HSQC spectral perturbations
220 observed in the presence of low molar equivalents of nucleosomes or dsDNA suggest similar
221 binding modes (**Figure 2—figure supplement 2B)**. Thus, the data identify two regions of
222 BARD1 (146-161 and 194-216) in the IDR adjacent to the enzymatic RING domains that bind
223 DNA when presented as free dsDNA or in the context of a nucleosome. The identified regions
224 are consistent with the H2A-Ub activity and nucleosome binding data presented above.
225
226 Having established that isolated BARD1 IDR fragments bind to free DNA and nucleosomes
227 similarly by NMR, we sought to observe the interactions within the context of an active
228 enzymatic complex. As such a complex would prove too large for NMR analysis, we turned to
229 targeted crosslinking of BRCA1/BARD1 to nucleosomal DNA. A photoactivatable crosslinker p-
230 Benzoyl-L-phenylalanine (Bpa) was incorporated using amber-codon suppression in *E. coli* at
231 individual locations throughout the BARD1 IDR in the context of RING-containing constructs
232 (L120Bpa, W146Bpa, Y180Bpa, A195Bpa and W218Bpa**; Figure 2—figure supplement 4A)**.
233 Due to the need to co-express a Bpa-specific aminoacyl tRNA transferase, we designed a
234 genetic fusion in which BRCA1 residues 1-104 are fused to BARD1 residues 26-221 through a
235 12-residue GlySer-linker (BRCA1-f-BARD1^{221}). Wild-type BRCA1-f-BARD1^{221} and Bpa-
236 incorporated mutants retained similar H2A-Ub activity to each other and to unfused
237 heterodimers **(Figure 2—figure supplement 4B)**. A nucleosome substrate with extra-

238 nucleosomal linker DNA that carried a fluorescent probe was used for crosslinking experiments
239 **(**NCP[185]; **Figure 2—figure supplement 4C)**. SDS-PAGE analysis of crosslinking reaction
240 products revealed shifted bands consistent with a covalent DNA-protein adduct for all Bpa
241 variants **(Figure 2C)**. Quantitation revealed enhanced crosslinks for the Bpa variants at BARD1
242 W146 and A195 positions, consistent with the NMR dsDNA binding data presented above
243 **(Figure 2C)**. Weaker crosslinks from the Y180 and W218 positions were comparable to
244 crosslinks observed from L120 that is located close to the RING domains and not expected to
245 contribute to productive DNA interactions. A similar crosslinking pattern was observed in
246 reactions containing free DNA **(Figure 2—figure supplement 4D)**. Together, the data support a
247 direct interaction between the BARD1 IDR and nucleosomal DNA in the context of an
248 enzymatically active complex.
249
250 **Contribution of DNA-binding to enhanced H2A-Ub activity**
251 Data presented thus far establish that the DNA-binding region of the BARD1 IDR is necessary
252 for high H2A-Ub activity, but is it sufficient? To address this question, we asked whether the
253 DNA-binding properties of full-length BARD1 can support H2A-Ub activity in the presence of
254 highly disruptive BARD1 RING histone-interface mutations **(**BARD1 P89A/W91A; **Figure 3A)**
255 (Hu et al., 2021; Witus, Burrell, et al., 2021). Although high-affinity nucleosome binding and
256 auto-ubiquitylation activity were retained, heterodimers containing full-length BARD1
257 (P89A/W91A) do not possess H2A-Ub activity **(Figure 3B, Figure 3—figure supplement 1A,**
258 **B)**. They also do not transfer Ub to other (off-target) histone sites **(Figure 3—figure**
259 **supplement 1C)**. Thus, the RING-histone interface is absolutely required for H2A-Ub activity,
260 while the DNA-binding properties of the BARD1 IDR serve to promote the formation of a high-
261 affinity complex that leads to enhanced H2A-Ub activity.
262

263 The disordered nature of the BARD1 DNA-binding region(s) raises the question of whether its
264 sequence identity is critical to support increased H2A-Ub activity. In other words, can any DNA-
265 binding region placed adjacent to the RING domain serve the same purpose? We generated a
266 chimeric BARD1 construct in which a previously identified DNA-binding region from the BRCA1
267 IDR (498-663) was appended onto the BARD1 RING (Mark et al., 2005). A heterodimer
268 composed of the BRCA1 RING and the BARD1 chimera supported increased H2A-Ub activity
269 as compared to the minimal RING/RING complex, but not to the levels of the native BARD1
270 sequence **(Figure 3C)**. The difference in activity is unlikely to be due solely to a difference in
271 DNA-binding affinity of the native BARD1 region versus the installed BRCA1-derived region, as
272 the measured affinities for nucleosomes are quite similar **(Figure 3—figure supplement 1D)**.
273 The small differences notwithstanding, the findings indicate that a major contributor to increased
274 H2A-Ub activity is the presence of a disordered, high-affinity DNA-binding region near the
275 enzymatic RING domains.
276
277 **Specialized DNA structures bind to the BARD1 IDR and inhibit H2A-Ub activity**
278 The BARD1 DNA-binding region enhances BRCA1/BARD1-mediated H2A-Ub activity by
279 interacting with nucleosomal DNA and increasing the affinity of the complex. It was previously
280 reported that this region of BARD1 preferentially binds to partly unwound DNA structures
281 (bubble-DNA) and homologous recombination (HR) intermediates (D-loop DNA) over double- or
282 single-stranded DNA (Zhao et al., 2017). The interactions with specialized DNA structures help
283 to promote HR through assembly of a functional complex consisting of BARD1, the
284 recombinase RAD51, and DNA. We hypothesized that the interaction between the BARD1
285 DNA-binding region and bubble- or D-loop DNA may alter its ability to interact with nucleosomal
286 DNA and consequently affect nucleosome binding and/or H2A-Ub activity. The molecular
287 features that BARD1 recognizes in bubble- and D-loop- DNA substrates are likely similar based

288 on the near-identical affinities of the BARD1-DNA complexes (Zhao et al., 2017), so we chose
289 to use the simpler bubble-DNA substrate in our assays.
290
291 Equal concentrations of DNA fragments containing various patterns of base-pair mismatch were
292 added to nucleosome ubiquitylation reactions carried out by full-length BRCA1/BARD1 **(Figure**
293 **4A, B and Figure 4—figure supplement 1A, B)**. Notably, among the DNA species tested, only
294 bubble-DNA substantially inhibited H2A-Ub activity. We hypothesized that the observed
295 inhibition is mediated through competing interactions between bubble-DNA and nucleosomal
296 DNA for binding to BARD1 141-216. Consistent with this notion, the minimal RING heterodimer
297 exhibits no sensitivity of its H2A-Ub activity to bubble-DNA **(Figure 4—figure supplement 1C,**
298 **D)**. Further support for a competitive binding mechanism is provided from UV-induced Bpa
299 crosslinking reactions that contained Bpa variants of $BRCA1^{RING}$-f-$BARD1^{221}$, nucleosomes, and
300 increasing concentrations of either bubble-DNA or dsDNA **(Figure 4C and Figure 4—figure**
301 **supplement 2).** Both types of DNA structure inhibited crosslink formation in a concentration-
302 dependent manner, but the bubble-DNA was substantially more effective.
303
304 To characterize the interactions between BARD1 141-216 and bubble-DNA, NMR spectra of
305 BARD1 IDR-DNA complexes bound to bubble-DNA and dsDNA fragments of similar sequence
306 and size were compared. CSPs and changes in dynamics within BARD1 194-216, the region we
307 previously showed to be the major site of dsDNA and nucleosomal DNA binding, were similar
308 between the bubble-DNA and dsDNA complexes **(Figure 4D and Figure 4—figure**
309 **supplement 3A-C)**. In addition, specific effects were produced by bubble-DNA: backbone
310 amide NMR resonances of BARD1 residues 143-157 exhibited severe broadening, with many
311 signals disappearing, indicative of large changes in chemical environment and/or dynamics. A
312 notable exception to the pattern of signals broadening beyond detection in this region is a large
313 CSP for the sidechain resonance of W146 that was observed only in the presence of bubble-

314 DNA **(Figure 4—figure supplement 3A, B)**. Further support for bubble-DNA-specific effects
315 comes from $^{1}H^{13}C$-HSQC spectra of BARD1 141-216. In the region of $^{1}H^{13}C$-HSQC spectra that
316 contains methyl group resonances, signals from residues within BARD1 143-157 exhibit large
317 CSPs that are not observed in the spectrum of dsDNA-bound BARD1 **(Figure 4E and Figure**
318 **4—figure supplement 3D)**. The data suggest that bubble-DNA binds to BARD1 194-216
319 similarly to dsDNA, but also strongly and specifically engages an additional DNA-binding site
320 near the beginning of the BARD1 IDR, namely residues 143-157. Consistent with this finding,
321 concomitant deletion of basic residues in both IDR regions ($BARD1^{\Delta 150-155/\Delta 194-216}$) was required
322 to alleviate H2A-Ub activity inhibition by bubble-DNA **(Figure 4F and Figure 4—figure**
323 **supplement 1E)**. Based on these findings, we conclude that BARD1 specifically recognizes
324 bubble-DNA via BARD1 residues 143-157 and that interactions with bubble-DNA can compete
325 with BARD1 IDR binding to nucleosomal DNA. This may lead to the observed repression of
326 BRCA1/BARD1 H2A-Ub activity in the presence of bubble-DNA competitor fragments.
327
328 **Extra-nucleosomal linker DNA enhances H2A ubiquitylation**
329 The extended domain topology of both BRCA1 and BARD1 raises the possibility of additional
330 interactions in higher-order chromatin substrates that are not present in minimal mono-
331 nucleosome substrates. For example, chromatin factors such as PRC2, LSD1, and VRK1
332 require linker DNA or adjacent nucleosome units for optimal binding and enzymatic activity
333 (Budziszewski et al., 2022; Kim et al., 2015; Poepsel et al., 2018; Wang et al., 2017). To test for
334 additional chromatin substrate requirements for BRCA1/BARD1-dependent H2A ubiquitylation,
335 nucleosome substrates with extra-nucleosomal linker DNA (NCP^{185}) and tri-nucleosomes (tri-
336 NCP) were used as substrates in H2A-Ub assays **(Figure 5A and Figure 5—figure**
337 **supplement 1A)**. In reactions performed using full-length BRCA1/BARD1, faster H2A-Ub
338 kinetics were observed for the NCP^{185} substrate with linker DNA compared to the minimal
339 NCP^{147} substrate **(Figure 5B)**. Notably, no additional increase in H2A-Ub activity was observed

340 for a tri-NCP substrate. The data are consistent with two conclusions: 1) the presence of linker
341 DNA enhances H2A-Ub activity and 2) functional interactions are limited to one mono-
342 nucleosome unit, at least in the absence of histone PTMs.
343
344 To confirm that the enhanced activity observed for the NCP^{185} and tri-NCP substrates described
345 above stem from the BARD1 IDR DNA-binding region, the H2A-Ub activity of the
346 $BRCA1^{RING}/BARD1^{216}$ truncation was tested **(Figure 5C)**. This species exhibited considerably
347 faster H2A-Ub kinetics on either a NCP^{185} or a tri-NCP substrate compared to a minimal NCP^{147}
348 substrate, again consistent with a dependence on the presence of linker DNA. To ask whether
349 the activity difference between the nucleosomes with and without linker DNA was due to
350 differences in binding affinity, we measured nucleosome binding affinity at two different ionic
351 strengths using the NCP^{147} and NCP^{185} substrates **(**100 mM vs. 150 mM NaCl; **Figure 5—figure**
352 **supplement 1B)**. Although nucleosome complexes exhibited considerably weaker binding (~5-
353 fold reduction) at higher buffer salt concentration, there was only a modest increase in binding
354 affinity with the NCP^{185} substrate at both ionic strengths. This behavior contrasts with other
355 chromatin factors that exhibit affinity and activity differences on the order of magnitudes in the
356 presence or absence of linker DNA and may reflect the different types of interactions (i.e.,
357 ordered vs disordered DNA-binding regions) (Kim et al., 2015; Wang et al., 2017, p. 2).
358 Together, our results indicate that the BARD1 DNA-binding region association with either
359 histone-associated nucleosomal DNA or extra-nucleosomal linker DNA leads to similar apparent
360 binding affinity. However, interactions with linker DNA support an additional enhancement of
361 H2A-Ub activity.
362
363 **H2A K15-Ub-mediated enhancement of BRCA1/BARD1 H2A-Ub activity**
364 In addition to the RING domains and the BARD1 DNA-binding region, the ordered C-terminal
365 domains (CTDs) of BARD1 bind to nucleosomes that contain both H2A K15-Ub and H4K20me0

366 (Dai et al., 2021; Hu et al., 2021). The BARD1 CTDs-nucleosome interactions serve to recruit
367 BRCA1/BARD1 to damaged chromatin to facilitate DNA DSB repair via HR (Becker et al., 2021;
368 Krais et al., 2021; Nakamura et al., 2019). The BARD1 CTDs use a histone-binding surface that
369 overlaps with the RING domain site, precluding binding of both to the same nucleosome face.
370 However, it was previously shown that nucleosomes containing H2A K15-Ub and H4K20me0
371 form a stronger complex with $BRCA1^{RING}$/$BARD1^{FL}$ and are better substrates for ubiquitylation of
372 H2A K127, thus implying that the RING domains and CTDs can simultaneously bind to opposite
373 faces of a nucleosome (Hu et al., 2021). We sought to further characterize the complexes using
374 our suite of BRCA1/BARD1 truncation constructs and chromatin substrates.
375
376 To ascertain the effects of pre-existing mono-Ub at H2A positions known to be ubiquitylated by
377 different ligases, homogenously mono-ubiquitylated nucleosomes containing ubiquitin
378 preinstalled at H2A positions K15, K119, or K127 were generated using a non-hydrolyzable
379 dichloroacetone crosslinker **(Figure 6—figure supplement 1A, B)** (Morgan et al., 2019). In
380 agreement with previous observations, ubiquitin preinstalled at H2A K15 uniquely increased the
381 H2A-Ub activity of full-length BRCA1/BARD1 **(Figure 6—figure supplement 1C, D)**. Ubiquitin
382 preinstalled at either H2A C-terminal position (K119 or K127) decreased BRCA1/BARD1-
383 dependent H2A-Ub activity, hinting at E3 exclusivity between BRCA1/BARD1 and RING1/PCGF
384 complexes that modify the H2A C-terminal tail. As expected, the BARD1 CTDs were required
385 for enhancement of BRCA1/BARD1-dependent H2A-Ub activity using H2A K15-Ub nucleosome
386 substrates **(Figure 6A)**. Importantly, this contrasts with our findings for unmodified nucleosome
387 substrates where the BARD1 CTDs are not required for enhanced H2A-Ub activity.
388
389 Are the DNA-binding properties of BARD1 important in the context of H2A K15-Ub nucleosome
390 substrates? Ubiquitylation reactions were carried out on H2A K15-Ub nucleosomes with a
391 selection of BARD1 truncation species. The internal BARD1 IDR deletion construct

392 (BRCA1^{RING}/BARD1$^{\Delta 140\text{-}270}$) exhibited decreased H2A-Ub kinetics compared with the
393 BRCA1^{RING}/BARD1^{FL} complex **(Figure 6A)**. Deletion of BARD1 140-270 still supported greater
394 activity than removal of the BARD1 CTDs (BRCA1^{RING}/BARD1$^{\Delta CTD}$). This indicates that BARD1-
395 DNA interactions are secondary to BARD1 CTDs-nucleosome binding on this substrate or can
396 be otherwise compensated by additional DNA-binding regions of BARD1. Additionally, the
397 histone-binding BARD1 RING mutant BRCA1^{RING}/BARD1$^{FL\text{-}P89A/W91A}$ does not support
398 BRCA1/BARD1-dependent H2A-Ub activity on H2A K15-Ub nucleosomes, supporting a model
399 where the BRCA1/BARD1 RINGs and CTDs bind to either face of a nucleosome. These
400 findings support a 'wrapped' complex model in which three points of contact between BARD1
401 and H2A K15-Ub nucleosomes (RING-histone, IDR-DNA, and CTDs-histone/Ub) are required
402 for full BRCA1/BARD1-dependent H2A-Ub activity **(Figure 7E)**.
403
404 To obtain information regarding complexes formed on unmodified mono-nucleosomes versus
405 H2A K15-Ub-modified nucleosomes, chemical crosslinking experiments were performed using
406 the amine-reactive crosslinkers DSS and BS3 **(Figure 6—figure supplement 2)**. To focus on
407 the interactions involving the BARD1 subunit, BRCA1^{RING}/BARD1^{FL} was used; products formed
408 in the crosslinking reactions were analyzed by mass spectrometry. Numerous intermolecular
409 crosslinks (judged by unique crosslinks and peptide spectral mapping counts) were detected
410 between the BARD1 CTDs and histones from nucleosomes containing H2A K15-Ub, while such
411 crosslinks were sparse in complexes composed of unmodified nucleosomes **(Figure 6B and**
412 **Figure 6—figure supplement 2C)**. The crosslinks are consistent with high-resolution structures
413 of the BARD1 CTDs bound to nucleosomes containing H2A K15-Ub and the lack of these in the
414 unmodified nucleosome reaction is consistent with the interaction being dependent on the
415 presence of Ub at H2A K15 **(Figure 6—figure supplement 2D)**. There was also increased
416 crosslinking between BARD1 RING and IDR domains to histones in samples containing H2A

417 K15-Ub nucleosomes **(Figure 6B, gray crosslinks and Figure 6—figure supplement 2C, E)**,
418 consistent with the reported higher binding affinity of that complex. Thus, binding of the BARD1
419 CTDs in response to the presence of H2A K15-Ub facilitates BARD1 RING and IDR interactions
420 that lead to the observed increase in H2A K127-Ub activity.
421
422 The BARD1 N-terminal RING domain and the CTD are separated by ~300 intrinsically
423 disordered residues, allowing for as much as 1000 Å of separation between the two ordered
424 domains. It is therefore possible that in addition to a 'wrapped' complex with H2A K15-Ub
425 nucleosomes, the BARD1 CTDs may anchor the heterodimeric complex by binding to one
426 nucleosome unit, while the RING domains are recruited to a nearby nucleosome unit on
427 chromatin to facilitate H2A-Ub activity. To test this possibility explicitly, asymmetric di-
428 nucleosome substrates (di-NCPs) where one nucleosome unit contained H2A K15-Ub ($H2A^{silent}$)
429 and an adjacent nucleosome unit contained unmodified H2A with a fluorophore conjugated near
430 its N-terminus to facilitate specific detection in a nucleosome ubiquitylation assay were
431 assembled **(**$H2A^{observe}$; **Figure 6C and Figure 6—figure supplement 1E-G)**. Using
432 $BRCA1^{RING}/BARD1^{FL}$ heterodimers, we observed that an asymmetric di-NCP substrate
433 containing H2A K15-Ub as $H2A^{silent}$ uniquely facilitates enhanced H2A-Ub modification of an
434 adjacent nucleosome unit containing unmodified H2A **(**$H2A^{observe}$; **Figure 6D and Figure 6—**
435 **figure supplement 1H)**. Removal of the BARD1 CTDs led to a large decrease in H2A-Ub
436 activity that was comparable to that of a di-NCP substrate where both nucleosome units contain
437 unmodified H2A. Consistent with observations made using H2A K15-Ub mono-nucleosomes,
438 $BRCA1^{RING}/BARD1^{FL\text{-}P89A/W91A}$ did not support H2A-Ub activity using asymmetric di-NCPs
439 **(Figure 6E)**. Additionally, deletion of BARD1 DNA-binding residues (Δ140-270) substantially
440 decreased H2A-Ub activity. The results support the formation of a higher-order chromatin
441 complex where BARD1 spans adjacent nucleosome units. The complex is mediated through

442 binding of the BRCA1/BARD1 RING domains and BARD1 CTDs to neighboring nucleosome
443 units and of the BARD1 IDR to intervening linker or nucleosomal DNA **(Figure 7F)**.
444
445 **Discussion**
446 Here, we describe distinct complexes between BRCA1/BARD1 and chromatin substrates that
447 depend on the status of histone PTMs on nucleosomes (e.g., unmodified or H2A K15-Ub)
448 **(Figure 7)**. Importantly, although the BARD1 CTDs are critical for enhanced interactions with
449 nucleosomes that contain H2A K15-Ub, they are dispensable for high-affinity interactions with
450 unmodified nucleosomes **(Figure 7C, D)**. Instead, additional interactions that enhance H2A-Ub
451 activity are mediated through a short and highly basic intrinsically disordered region of BARD1
452 (primarily residues 194-216) adjacent to the enzymatic RING domains that engages
453 nucleosomal and extra-nucleosomal linker DNA. These strong, electrostatic-based interactions
454 increase the binding affinity of the complex from the micromolar to the nanomolar binding
455 regime that is likely critical to support the physiological functions of BRCA1/BARD1 on
456 chromatin. Our findings indicate that DNA binding plays an auxiliary role in the ability of
457 BRCA1/BARD1 to ubiquitylate H2A by boosting the affinity of the Ub ligase/nucleosome
458 complex. Supporting this, a BARD1 RING-domain mutant (BARD1 P89A/W91A) that disrupts
459 histone binding is unable to support H2A-Ub activity with any chromatin substrate tested despite
460 retaining strong nucleosome binding affinity and intrinsic Ub ligase activity. This indicates that
461 high-affinity binding to nucleosomal DNA by the BARD1 IDR is not sufficient for H2A-Ub activity,
462 while the positioning of the RING domains on the histone surface is absolutely required.
463 Therefore, BARD1 P89A/W91A may constitute a separation-of-function mutant for cellular
464 studies to investigate the specific roles of BRCA1/BARD1-dependent H2A-Ub.
465
466 BRCA1/BARD1 functions in many distinct chromatin-associated complexes and also binds to
467 nucleic acids (Mark et al., 2005; Savage & Harkin, 2015; Zhao et al., 2017). Highlighting the

468 importance of other BRCA1/BARD1 binding factors, we identified specific DNA structures
469 (bubble-DNA) that inhibit nucleosome binding and H2A-Ub activity by binding to the BARD1 IDR
470 and competing with nucleosome binding. The recognition mechanism is likely similar for D-loop
471 DNA structures that are intermediates in HR (Zhao et al., 2017), and possibly R-loop structures
472 that have similar chemical properties (Santos-Pereira & Aguilera, 2015). It is possible that
473 binding of the BARD1 IDR region to either nucleosomal DNA or specialized nucleic acid
474 structures serves to control its spatial and temporal involvement in HR and other processes
475 where such specialized DNA structures may be present (e.g., stalled replication fork protection,
476 R-loop resolution) (Hatchi et al., 2015; Schlacher et al., 2012). Additionally, BRCA1/BARD1 is
477 present in higher-order protein assemblies that are known to bind to chromatin via distinct
478 nucleosome interfaces that may be formed by other proteins in the complex (Belotserkovskaya
479 et al., 2020, p. 2; Bochar et al., 2000; Huen et al., 2010; Savage & Harkin, 2015). Understanding
480 the combined binding contributions of BRCA1/BARD1 and other proteins in such complexes to
481 nucleosome association and H2A-Ub activity is an important future goal.
482
483 BRCA1/BARD1 nucleosome binding and H2A-Ub activity is also responsive to pre-existing
484 histone PTMs, as in the case of H2A K15-Ub. In addition to a wrapped complex where the
485 BARD1 CTDs and BRCA1/BARD1 RINGs occupy opposite nucleosome faces, we provide
486 evidence for a complex where the BARD1 CTDs and the enzymatic RING domains occupy
487 adjacent nucleosome units **(Figure 7E, F)**. The BARD1 IDR region enables extensive
488 separation between the enzymatic RING domains and BARD1 CTDs while forming high-affinity
489 interactions with nucleosomal DNA. This may allow the RING domains to reach nucleosome
490 units considerably further away than an adjacent unit while anchored to chromatin via the
491 BARD1 CTDs. This ability could lead to BRCA1/BARD1-dependent H2A-Ub of multiple
492 nucleosomes in the vicinity of a H2A K15-Ub anchor nucleosome. Additionally, the ability to
493 reach across nucleosome units in chromatin provides a platform to scaffold unique higher-order

494 complexes across long molecular distances. As H2A K15-Ub is a highly specific mark of DNA
495 damage, it is unlikely to serve as a universal recruitment signal for other BRCA1/BARD1-
496 dependent processes such as transcriptional regulation. An important unanswered question is
497 how other histone PTMs influence the chromatin binding and H2A-Ub activity of
498 BRCA1/BARD1. Previously, we observed that methylation at H3 K79, a mark associated with
499 actively transcribed chromatin, inhibits BRCA1/BARD1-mediated H2A-Ub activity (Witus,
500 Burrell, et al., 2021). This may be attributable to the location of H3 K79 near the BARD1-histone
501 interface. A comprehensive understanding of histone PTMs that influence BRCA1/BARD1
502 nucleosome binding, higher-order chromatin complex formation, and H2A-Ub activity will
503 provide valuable insight into its functions and regulation in different biological processes.
504
505 In sum, our results establish an extensive multivalent network of interactions that facilitate
506 BRCA1/BARD1 chromatin binding and H2A-Ub activity. These interactions are likely critical for
507 many functions of BRCA1/BARD1 in the nucleus that are not limited to its H2A-Ub activity and
508 may be disrupted by mutations that cause cancer.
509
510 **Ideas and Speculation:**
511 Because BRCA1/BARD1 serves as a large protein interaction hub that forms many distinct
512 complexes, it is possible that the accessibility of DNA-binding regions in BARD1 (and perhaps in
513 BRCA1) is determined by the landscape of binding partners with which it is associated. On this
514 point, we observed that full-length BRCA1/BARD1 has lower H2A-Ub activity than complexes
515 containing truncated BRCA1 (Δ11q or RING). This is despite the presence of additional DNA-
516 binding regions within the BRCA1 IDR that can support increased H2A-Ub activity. A possible
517 explanation is a competition among the various DNA-binding regions from BRCA1 and BARD1
518 for binding to nucleosomes, with binding of the BRCA1 region resulting in lower H2A-Ub activity.
519 Alternatively, possible inhibitory interactions between BRCA1 and BARD1 subunits might be

520 alleviated upon BRCA1 truncation. Occupancy of different regions of BRCA1 and BARD1 by
521 unique binding partners may occlude certain nucleosome-binding regions, resulting in inhibition
522 or enhancement of chromatin binding and H2A-Ub activity. Further investigation into chromatin
523 complexes containing full-length BRCA1/BARD1 and the many protein assemblies and binding
524 partners that are required to execute its cellular functions is warranted.
525

526 **Acknowledgements**

527 We thank K. Luger (University of Colorado Boulder) for sharing plasmids for the 147-bp and
528 NLE-trimer '601' DNA, S. Tan (Penn State University) for sharing the plasmid for the 185-bp
529 '601' DNA, and G. Debelouchina (UC San Diego) for the MMTV DNA plasmid. We thank D.
530 Veelser for providing access to equipment, and M. Morgan for insights into dichloroacetone
531 crosslinking of H2A-Ub. S.R.W., L.M.T., K.EK., P.S.B., and R.E.K. were supported by the NIH
532 (R01CA260834). R.E.K. is the Edmond H. Fischer/Washington Research Foundation Endowed
533 Chair in Biochemistry. This work and A.Z. was supported in part by the University of
534 Washington's Proteomics Resource (UWPR95794). A.Z. and T.N.D. were also supported by the
535 NIH (P41GM103533). W.Z. was supported by a Young Investigator Award from Max and Minnie
536 Tomerlin Voelcker Fund, the Cancer Prevention and Research Institute of Texas (RP210102),
537 and the NIH (R01GM141091). D.B.W. was supported by the NIH (R00-HD090201).
538

539 **Author Contributions**

540 S.R.W., W.Z., P.S.B., and R.E.K. conceived of the study. S.R.W., L.M.T., and K.E.K. performed
541 experiments and analyzed data. D.B.W. analyzed data. A.Z. performed chemical crosslinking
542 and mass spectrometry and associated data processing under the supervision of T.N.D. S.R.W.
543 wrote the initial draft of the manuscript and generated all figures. The final manuscript was
544 written by S.R.W., P.S.B., and R.E.K., with input from all co-authors.
545

Competing Interests Statement

The authors of this article declare no competing interests.

References

Alenezi, W. M., Fierheller, C. T., Recio, N., & Tonin, P. N. (2020). Literature Review of BARD1 as a Cancer Predisposing Gene with a Focus on Breast and Ovarian Cancers. *Genes*, *11*(8). https://doi.org/10.3390/genes11080856

Becker, J. R., Clifford, G., Bonnet, C., Groth, A., Wilson, M. D., & Chapman, J. R. (2021). BARD1 reads H2A lysine 15 ubiquitination to direct homologous recombination. *Nature*, *596*(7872), 433–437. https://doi.org/10.1038/s41586-021-03776-w

Belotserkovskaya, R., Raga Gil, E., Lawrence, N., Butler, R., Clifford, G., Wilson, M. D., & Jackson, S. P. (2020). PALB2 chromatin recruitment restores homologous recombination in BRCA1-deficient cells depleted of 53BP1. *Nature Communications*, *11*(1), 819. https://doi.org/10.1038/s41467-020-14563-y

Bochar, D. A., Wang, L., Beniya, H., Kinev, A., Xue, Y., Lane, W. S., Wang, W., Kashanchi, F., & Shiekhattar, R. (2000). BRCA1 Is Associated with a Human SWI/SNF-Related Complex: Linking Chromatin Remodeling to Breast Cancer. *Cell*, *102*(2), 257–265. https://doi.org/10.1016/S0092-8674(00)00030-1

Brzovic, P. S., Keeffe, J. R., Nishikawa, H., Miyamoto, K., Fox, D., 3rd, Fukuda, M., Ohta, T., & Klevit, R. (2003). Binding and recognition in the assembly of an active BRCA1/BARD1 ubiquitin-ligase complex. *Proceedings of the National Academy of Sciences of the United States of America*, *100*(10), 5646–5651. PubMed. https://doi.org/10.1073/pnas.0836054100

Brzovic, P. S., Rajagopal, P., Hoyt, D. W., King, M. C., & Klevit, R. E. (2001). Structure of a BRCA1-BARD1 heterodimeric RING-RING complex. *Nature Structural Biology*, *8*(10), 833–837. PubMed. https://doi.org/10.1038/nsb1001-833

Budziszewski, G. R., Zhao, Y., Spangler, C. J., Kedziora, K. M., Williams, M. R., Azzam, D. N., Skrajna, A., Koyama, Y., Cesmat, A. P., Simmons, H. C., Arteaga, E. C., Strauss, J. D., Kireev, D., & McGinty, R. K. (2022). Multivalent DNA and nucleosome acidic patch interactions specify VRK1 mitotic localization and activity. *Nucleic Acids Research*, *50*(8), 4355–4371. https://doi.org/10.1093/nar/gkac198

Chambers, M. C., Maclean, B., Burke, R., Amodei, D., Ruderman, D. L., Neumann, S., Gatto, L., Fischer, B., Pratt, B., Egertson, J., Hoff, K., Kessner, D., Tasman, N., Shulman, N., Frewen, B., Baker, T. A., Brusniak, M.-Y., Paulse, C., Creasy, D., … Mallick, P. (2012). A cross-platform toolkit for mass spectrometry and proteomics. *Nature Biotechnology*, *30*(10), 918–920. https://doi.org/10.1038/nbt.2377

Chin Jason W., Martin Andrew B., King David S., Wang Lei, & Schultz Peter G. (2002). Addition of a photocrosslinking amino acid to the genetic code of Escherichia coli. *Proceedings of the National Academy of Sciences*, *99*(17), 11020–11024. https://doi.org/10.1073/pnas.172226299

Christensen, D. E., Brzovic, P. S., & Klevit, R. E. (2007). E2-BRCA1 RING interactions dictate synthesis of mono- or specific polyubiquitin chain linkages. *Nature Structural & Molecular Biology*, *14*(10), 941–948. https://doi.org/10.1038/nsmb1295

589 Dai, L., Dai, Y., Han, J., Huang, Y., Wang, L., Huang, J., & Zhou, Z. (2021). Structural insight
590 into BRCA1-BARD1 complex recruitment to damaged chromatin. *Molecular Cell*, *81*(13),
591 2765-2777.e6. https://doi.org/10.1016/j.molcel.2021.05.010

592 Dao, H. T., Dul, B. E., Dann, G. P., Liszczak, G. P., & Muir, T. W. (2020). A basic motif
593 anchoring ISWI to nucleosome acidic patch regulates nucleosome spacing. *Nature*
594 *Chemical Biology*, *16*(2), 134–142. https://doi.org/10.1038/s41589-019-0413-4

595 Densham, R. M., Garvin, A. J., Stone, H. R., Strachan, J., Baldock, R. A., Daza-Martin, M.,
596 Fletcher, A., Blair-Reid, S., Beesley, J., Johal, B., Pearl, L. H., Neely, R., Keep, N. H.,
597 Watts, F. Z., & Morris, J. R. (2016). Human BRCA1-BARD1 ubiquitin ligase activity
598 counteracts chromatin barriers to DNA resection. *Nature Structural & Molecular Biology*,
599 *23*(7), 647–655. PubMed. https://doi.org/10.1038/nsmb.3236

600 Densham, R. M., & Morris, J. R. (2019). Moving Mountains—The BRCA1 Promotion of DNA
601 Resection. *Frontiers in Molecular Biosciences*, *6*, 79.
602 https://doi.org/10.3389/fmolb.2019.00079

603 Dyer, P. N., Edayathumangalam, R. S., White, C. L., Bao, Y., Chakravarthy, S., Muthurajan, U.
604 M., & Luger, K. (2003). Reconstitution of Nucleosome Core Particles from Recombinant
605 Histones and DNA. In *Methods in Enzymology* (Vol. 375, pp. 23–44). Academic Press.
606 https://doi.org/10.1016/S0076-6879(03)75002-2

607 Eng, J. K., Jahan, T. A., & Hoopmann, M. R. (2013). Comet: An open-source MS/MS sequence
608 database search tool. *PROTEOMICS*, *13*(1), 22–24.
609 https://doi.org/10.1002/pmic.201200439

610 Gudmundsdottir, K., & Ashworth, A. (2006). The roles of BRCA1 and BRCA2 and associated
611 proteins in the maintenance of genomic stability. *Oncogene*, *25*(43), 5864–5874.
612 https://doi.org/10.1038/sj.onc.1209874

613 Hatchi, E., Skourti-Stathaki, K., Ventz, S., Pinello, L., Yen, A., Kamieniarz-Gdula, K., Dimitrov,
614 S., Pathania, S., McKinney, K. M., Eaton, M. L., Kellis, M., Hill, S. J., Parmigiani, G.,
615 Proudfoot, N. J., & Livingston, D. M. (2015). BRCA1 recruitment to transcriptional pause
616 sites is required for R-loop-driven DNA damage repair. *Molecular Cell*, *57*(4), 636–647.
617 PubMed. https://doi.org/10.1016/j.molcel.2015.01.011

618 Hoopmann, M. R., Zelter, A., Johnson, R. S., Riffle, M., MacCoss, M. J., Davis, T. N., & Moritz,
619 R. L. (2015). Kojak: Efficient Analysis of Chemically Cross-Linked Protein Complexes.
620 *Journal of Proteome Research*, *14*(5), 2190–2198. https://doi.org/10.1021/pr501321h

621 Hsu, P. L., Shi, H., Leonen, C., Kang, J., Chatterjee, C., & Zheng, N. (2019). Structural Basis of
622 H2B Ubiquitination-Dependent H3K4 Methylation by COMPASS. *Molecular Cell*, *76*(5),
623 712-723.e4. https://doi.org/10.1016/j.molcel.2019.10.013

624 Hu, Q., Botuyan, M. V., Zhao, D., Cui, G., Mer, E., & Mer, G. (2021). Mechanisms of BRCA1–
625 BARD1 nucleosome recognition and ubiquitylation. *Nature*, *596*(7872), 438–443.
626 https://doi.org/10.1038/s41586-021-03716-8

627 Huen, M. S. Y., Sy, S. M. H., & Chen, J. (2010). BRCA1 and its toolbox for the maintenance of
628 genome integrity. *Nature Reviews Molecular Cell Biology*, *11*(2), 138–148.
629 https://doi.org/10.1038/nrm2831

630 Kalb, R., Mallery, D. L., Larkin, C., Huang, J. T. J., & Hiom, K. (2014). BRCA1 is a histone-H2A-
631 specific ubiquitin ligase. *Cell Reports*, *8*(4), 999–1005. PubMed.
632 https://doi.org/10.1016/j.celrep.2014.07.025

Käll, L., Canterbury, J. D., Weston, J., Noble, W. S., & MacCoss, M. J. (2007). Semi-supervised learning for peptide identification from shotgun proteomics datasets. *Nature Methods*, *4*(11), 923–925. https://doi.org/10.1038/nmeth1113

Katoh, K., & Standley, D. M. (2013). MAFFT Multiple Sequence Alignment Software Version 7: Improvements in Performance and Usability. *Molecular Biology and Evolution*, *30*(4), 772–780. https://doi.org/10.1093/molbev/mst010

Kim, S.-A., Chatterjee, N., Jennings, M. J., Bartholomew, B., & Tan, S. (2015). Extranucleosomal DNA enhances the activity of the LSD1/CoREST histone demethylase complex. *Nucleic Acids Research*, *43*(10), 4868–4880. https://doi.org/10.1093/nar/gkv388

Kjaergaard, M., & Poulsen, F. M. (2011). Sequence correction of random coil chemical shifts: Correlation between neighbor correction factors and changes in the Ramachandran distribution. *Journal of Biomolecular NMR*, *50*(2), 157–165. https://doi.org/10.1007/s10858-011-9508-2

Kolas Nadine K., Chapman J. Ross, Nakada Shinichiro, Ylanko Jarkko, Chahwan Richard, Sweeney Frédéric D., Panier Stephanie, Mendez Megan, Wildenhain Jan, Thomson Timothy M., Pelletier Laurence, Jackson Stephen P., & Durocher Daniel. (2007). Orchestration of the DNA-Damage Response by the RNF8 Ubiquitin Ligase. *Science*, *318*(5856), 1637–1640. https://doi.org/10.1126/science.1150034

Krais, J. J., & Johnson, N. (2020). BRCA1 Mutations in Cancer: Coordinating Deficiencies in Homologous Recombination with Tumorigenesis. *Cancer Research*, *80*(21), 4601–4609. https://doi.org/10.1158/0008-5472.CAN-20-1830

Krais, J. J., Wang, Y., Patel, P., Basu, J., Bernhardy, A. J., & Johnson, N. (2021). RNF168-mediated localization of BARD1 recruits the BRCA1-PALB2 complex to DNA damage. *Nature Communications*, *12*(1), 5016. https://doi.org/10.1038/s41467-021-25346-4

Lazar, G. A., Desjarlais, J. R., & Handel, T. M. (1997). De novo design of the hydrophobic core of ubiquitin. *Protein Science : A Publication of the Protein Society*, *6*(6), 1167–1178. PubMed. https://doi.org/10.1002/pro.5560060605

Lee, Y.-T., Gibbons, G., Lee, S. Y., Nikolovska-Coleska, Z., & Dou, Y. (2015). One-pot refolding of core histones from bacterial inclusion bodies allows rapid reconstitution of histone octamer. *Protein Expression and Purification*, *110*, 89–94. PubMed. https://doi.org/10.1016/j.pep.2015.02.007

Lorick, K. L., Jensen, J. P., Fang, S., Ong, A. M., Hatakeyama, S., & Weissman, A. M. (1999). RING fingers mediate ubiquitin-conjugating enzyme (E2)-dependent ubiquitination. *Proceedings of the National Academy of Sciences*, *96*(20), 11364. https://doi.org/10.1073/pnas.96.20.11364

Lowary, P. T., & Widom, J. (1998). New DNA sequence rules for high affinity binding to histone octamer and sequence-directed nucleosome positioning11Edited by T. Richmond. *Journal of Molecular Biology*, *276*(1), 19–42. https://doi.org/10.1006/jmbi.1997.1494

Luger, K., Rechsteiner, T. J., & Richmond, T. J. (1999). Preparation of nucleosome core particle from recombinant histones. *Methods in Enzymology*, *304*, 3–19. https://doi.org/10.1016/s0076-6879(99)04003-3

Mark, W.-Y., Liao, J. C. C., Lu, Y., Ayed, A., Laister, R., Szymczyna, B., Chakrabartty, A., & Arrowsmith, C. H. (2005). Characterization of segments from the central region of BRCA1: An intrinsically disordered scaffold for multiple protein-protein and protein-DNA

interactions? *Journal of Molecular Biology*, *345*(2), 275–287. PubMed. https://doi.org/10.1016/j.jmb.2004.10.045

Masuda, T., Xu, X., Dimitriadis, E. K., Lahusen, T., & Deng, C.-X. (2016). “DNA Binding Region” of BRCA1 Affects Genetic Stability through modulating the Intra-S-Phase Checkpoint. *International Journal of Biological Sciences*, *12*(2), 133–143. PubMed. https://doi.org/10.7150/ijbs.14242

Mattiroli, F., Vissers, J. H. A., van Dijk, W. J., Ikpa, P., Citterio, E., Vermeulen, W., Marteijn, J. A., & Sixma, T. K. (2012). RNF168 ubiquitinates K13-15 on H2A/H2AX to drive DNA damage signaling. *Cell*, *150*(6), 1182–1195. https://doi.org/10.1016/j.cell.2012.08.005

McGinty, R. K., Henrici, R. C., & Tan, S. (2014). Crystal structure of the PRC1 ubiquitylation module bound to the nucleosome. *Nature*, *514*(7524), 591–596. PubMed. https://doi.org/10.1038/nature13890

McGinty, R. K., & Tan, S. (2016). Recognition of the nucleosome by chromatin factors and enzymes. *Current Opinion in Structural Biology*, *37*, 54–61. https://doi.org/10.1016/j.sbi.2015.11.014

McGinty, R. K., & Tan, S. (2021). Principles of nucleosome recognition by chromatin factors and enzymes. *Catalysis and Regulation ● Protein Nucleic Acid Interactions*, *71*, 16–26. https://doi.org/10.1016/j.sbi.2021.05.006

McGuffin, L. J., Bryson, K., & Jones, D. T. (2000). The PSIPRED protein structure prediction server. *Bioinformatics*, *16*(4), 404–405. https://doi.org/10.1093/bioinformatics/16.4.404

Morgan, M., Jbara, M., Brik, A., & Wolberger, C. (2019). Chapter One—Semisynthesis of ubiquitinated histone H2B with a native or nonhydrolyzable linkage. In M. Hochstrasser (Ed.), *Methods in Enzymology* (Vol. 618, pp. 1–27). Academic Press. https://doi.org/10.1016/bs.mie.2019.01.003

Morgan Michael T., Haj-Yahya Mahmood, Ringel Alison E., Bandi Prasanthi, Brik Ashraf, & Wolberger Cynthia. (2016). Structural basis for histone H2B deubiquitination by the SAGA DUB module. *Science*, *351*(6274), 725–728. https://doi.org/10.1126/science.aac5681

Mullan, P. B., Quinn, J. E., & Harkin, D. P. (2006). The role of BRCA1 in transcriptional regulation and cell cycle control. *Oncogene*, *25*(43), 5854–5863. https://doi.org/10.1038/sj.onc.1209872

Nakamura, K., Saredi, G., Becker, J. R., Foster, B. M., Nguyen, N. V., Beyer, T. E., Cesa, L. C., Faull, P. A., Lukauskas, S., Frimurer, T., Chapman, J. R., Bartke, T., & Groth, A. (2019). H4K20me0 recognition by BRCA1–BARD1 directs homologous recombination to sister chromatids. *Nature Cell Biology*, *21*(3), 311–318. https://doi.org/10.1038/s41556-019-0282-9

Poepsel, S., Kasinath, V., & Nogales, E. (2018). Cryo-EM structures of PRC2 simultaneously engaged with two functionally distinct nucleosomes. *Nature Structural & Molecular Biology*, *25*(2), 154–162. https://doi.org/10.1038/s41594-018-0023-y

Riffle, M., Jaschob, D., Zelter, A., & Davis, T. N. (2016). ProXL (Protein Cross-Linking Database): A Platform for Analysis, Visualization, and Sharing of Protein Cross-Linking Mass Spectrometry Data. *Journal of Proteome Research*, *15*(8), 2863–2870. https://doi.org/10.1021/acs.jproteome.6b00274

Riffle, M., Jaschob, D., Zelter, A., & Davis, T. N. (2019). Proxl (Protein Cross-Linking Database): A Public Server, QC Tools, and Other Major Updates. *Journal of Proteome Research*, *18*(2), 759–764. https://doi.org/10.1021/acs.jproteome.8b00726

Santos-Pereira, J. M., & Aguilera, A. (2015). R loops: New modulators of genome dynamics and function. *Nature Reviews Genetics*, *16*(10), 583–597. https://doi.org/10.1038/nrg3961

Savage, K. I., & Harkin, D. P. (2015). BRCA1, a “complex” protein involved in the maintenance of genomic stability. *The FEBS Journal*, *282*(4), 630–646. https://doi.org/10.1111/febs.13150

Schlacher, K., Wu, H., & Jasin, M. (2012). A Distinct Replication Fork Protection Pathway Connects Fanconi Anemia Tumor Suppressors to RAD51-BRCA1/2. *Cancer Cell*, *22*(1), 106–116. https://doi.org/10.1016/j.ccr.2012.05.015

Scully, R., Chen, J., Ochs, R. L., Keegan, K., Hoekstra, M., Feunteun, J., & Livingston, D. M. (1997). Dynamic Changes of BRCA1 Subnuclear Location and Phosphorylation State Are Initiated by DNA Damage. *Cell*, *90*(3), 425–435. https://doi.org/10.1016/S0092-8674(00)80503-6

Simons, A. M., Horwitz, A. A., Starita, L. M., Griffin, K., Williams, R. S., Glover, J. N. M., & Parvin, J. D. (2006). BRCA1 DNA-Binding Activity Is Stimulated by BARD1. *Cancer Research*, *66*(4), 2012–2018. https://doi.org/10.1158/0008-5472.CAN-05-3296

Sobhian Bijan, Shao Genze, Lilli Dana R., Culhane Aedín C., Moreau Lisa A., Xia Bing, Livingston David M., & Greenberg Roger A. (2007). RAP80 Targets BRCA1 to Specific Ubiquitin Structures at DNA Damage Sites. *Science*, *316*(5828), 1198–1202. https://doi.org/10.1126/science.1139516

Stewart, M. D., Zelin, E., Dhall, A., Walsh, T., Upadhyay, E., Corn, J. E., Chatterjee, C., King, M.-C., & Klevit, R. E. (2018). BARD1 is necessary for ubiquitylation of nucleosomal histone H2A and for transcriptional regulation of estrogen metabolism genes. *Proceedings of the National Academy of Sciences of the United States of America*, *115*(6), 1316–1321. PubMed. https://doi.org/10.1073/pnas.1715467115

Tan, W., Murphy, V. J., Charron, A., van Twest, S., Sharp, M., Constantinou, A., Parker, M. W., Crismani, W., Bythell-Douglas, R., & Deans, A. J. (2020). Preparation and purification of mono-ubiquitinated proteins using Avi-tagged ubiquitin. *PLOS ONE*, *15*(2), e0229000. https://doi.org/10.1371/journal.pone.0229000

Tarsounas, M., & Sung, P. (2020). The antitumorigenic roles of BRCA1–BARD1 in DNA repair and replication. *Nature Reviews Molecular Cell Biology*, *21*(5), 284–299. https://doi.org/10.1038/s41580-020-0218-z

Uckelmann, M., Densham, R. M., Baas, R., Winterwerp, H. H. K., Fish, A., Sixma, T. K., & Morris, J. R. (2018). USP48 restrains resection by site-specific cleavage of the BRCA1 ubiquitin mark from H2A. *Nature Communications*, *9*(1), 229. https://doi.org/10.1038/s41467-017-02653-3

Virtanen, P., Gommers, R., Oliphant, T. E., Haberland, M., Reddy, T., Cournapeau, D., Burovski, E., Peterson, P., Weckesser, W., Bright, J., van der Walt, S. J., Brett, M., Wilson, J., Millman, K. J., Mayorov, N., Nelson, A. R. J., Jones, E., Kern, R., Larson, E., … SciPy 1.0 Contributors. (2020). SciPy 1.0: Fundamental algorithms for scientific computing in Python. *Nature Methods*, *17*(3), 261–272. https://doi.org/10.1038/s41592-019-0686-2

Vizcaíno, J. A., Côté, R., Reisinger, F., M. Foster, J., Mueller, M., Rameseder, J., Hermjakob, H., & Martens, L. (2009). A guide to the Proteomics Identifications Database proteomics data repository. *PROTEOMICS*, *9*(18), 4276–4283. https://doi.org/10.1002/pmic.200900402

Wang, X., Paucek, R. D., Gooding, A. R., Brown, Z. Z., Ge, E. J., Muir, T. W., & Cech, T. R. (2017). Molecular analysis of PRC2 recruitment to DNA in chromatin and its inhibition by RNA. *Nature Structural & Molecular Biology*, *24*(12), 1028–1038. https://doi.org/10.1038/nsmb.3487

Witus, S. R., Burrell, A. L., Farrell, D. P., Kang, J., Wang, M., Hansen, J. M., Pravat, A., Tuttle, L. M., Stewart, M. D., Brzovic, P. S., Chatterjee, C., Zhao, W., DiMaio, F., Kollman, J. M., & Klevit, R. E. (2021). BRCA1/BARD1 site-specific ubiquitylation of nucleosomal H2A is directed by BARD1. *Nature Structural & Molecular Biology*, *28*(3), 268–277. https://doi.org/10.1038/s41594-020-00556-4

Witus, S. R., Stewart, M. D., & Klevit, R. E. (2021). The BRCA1/BARD1 ubiquitin ligase and its substrates. *Biochemical Journal*, 3467–3483. https://doi.org/10.1042/BCJ20200864

Witus, S. R., Zhao, W., Brzovic, P. S., & Klevit, R. E. (2022). BRCA1/BARD1 is a nucleosome reader and writer. *Trends in Biochemical Sciences*. https://doi.org/10.1016/j.tibs.2022.03.001

Worden, E. J., Hoffmann, N. A., Hicks, C. W., & Wolberger, C. (2019). Mechanism of Cross-talk between H2B Ubiquitination and H3 Methylation by Dot1L. *Cell*, *176*(6), 1490-1501.e12. PubMed. https://doi.org/10.1016/j.cell.2019.02.002

Worden, E. J., Zhang, X., & Wolberger, C. (2020). Structural basis for COMPASS recognition of an H2B-ubiquitinated nucleosome. *ELife*, *9*, e53199. https://doi.org/10.7554/eLife.53199

Zelter, A., Bonomi, M., Kim, J. ook, Umbreit, N. T., Hoopmann, M. R., Johnson, R., Riffle, M., Jaschob, D., MacCoss, M. J., Moritz, R. L., & Davis, T. N. (2015). The molecular architecture of the Dam1 kinetochore complex is defined by cross-linking based structural modelling. *Nature Communications*, *6*(1), 8673. https://doi.org/10.1038/ncomms9673

Zhao, W., Steinfeld, J. B., Liang, F., Chen, X., Maranon, D. G., Jian Ma, C., Kwon, Y., Rao, T., Wang, W., Sheng, C., Song, X., Deng, Y., Jimenez-Sainz, J., Lu, L., Jensen, R. B., Xiong, Y., Kupfer, G. M., Wiese, C., Greene, E. C., & Sung, P. (2017). BRCA1-BARD1 promotes RAD51-mediated homologous DNA pairing. *Nature*, *550*(7676), 360–365. PubMed. https://doi.org/10.1038/nature24060

Zhu, G., Xia, Y., Nicholson, L. K., & Sze, K. H. (2000). Protein Dynamics Measurements by TROSY-Based NMR Experiments. *Journal of Magnetic Resonance*, *143*(2), 423–426. https://doi.org/10.1006/jmre.2000.2022

Zhu, Q., Hoong, N., Aslanian, A., Hara, T., Benner, C., Heinz, S., Miga, K. H., Ke, E., Verma, S., Soroczynski, J., Yates, J. R., Hunter, T., & Verma, I. M. (2018). Heterochromatin-Encoded Satellite RNAs Induce Breast Cancer. *Molecular Cell*, *70*(5), 842-853.e7. https://doi.org/10.1016/j.molcel.2018.04.023

Zhu, Q., Pao, G. M., Huynh, A. M., Suh, H., Tonnu, N., Nederlof, P. M., Gage, F. H., & Verma, I. M. (2011). BRCA1 tumour suppression occurs via heterochromatin-mediated silencing. *Nature*, *477*(7363), 179–184. https://doi.org/10.1038/nature10371

Figures

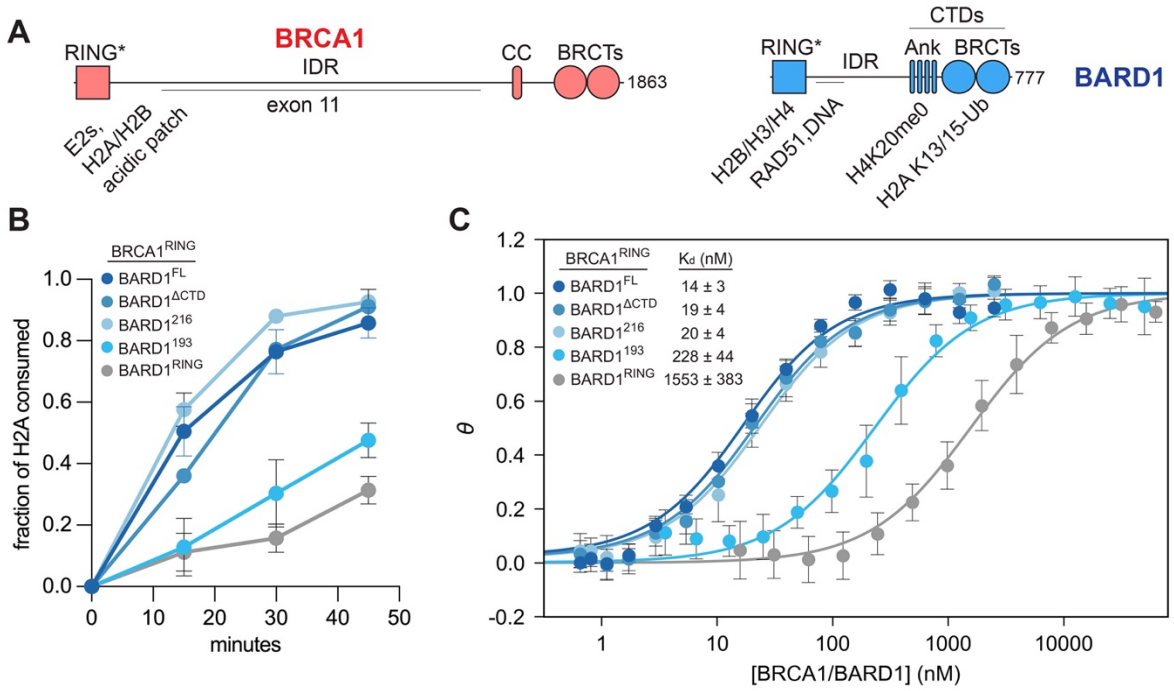

Figure 1. Contributions of BARD1 regions to nucleosome binding and H2A-Ub activity. **(A)** Domain organization of BRCA1 and BARD1. The domain names are indicated above the cartoons (RING, really interesting new gene; IDR, intrinsically disordered region; CC, coiled-coil; BRCT, BRCA1 C-terminal; Ank, Ankyrin repeat domain; CTD, C-terminal domain). Binding sites of interacting partners previously described and relevant to this work are indicated below the domain illustrations. The heterodimeric interface is denoted by an asterisk. **(B)** Quantification of time-course nucleosome H2A-Ub assays using the indicated BRCA1/BARD1 truncations. Data show the mean; error bars are ± 1-s.d. of n=3 independent experiments. **(C)** Comparison of nucleosome binding affinity from fluorescence-quenching based measurements using the indicated BRCA1/BARD1 constructs. Data show the mean; error bars are ± 1-s.d. of n=4 independent experiments. The reported difference in affinities to $BRCA1^{RING}/BARD1^{RING}$ is likely underestimated, as the minimal RING/RING heterodimer binding data was collected at a lower ionic strength than the rest of the constructs to obtain well-behaved binding data (50 mM vs. 100 mM NaCl).

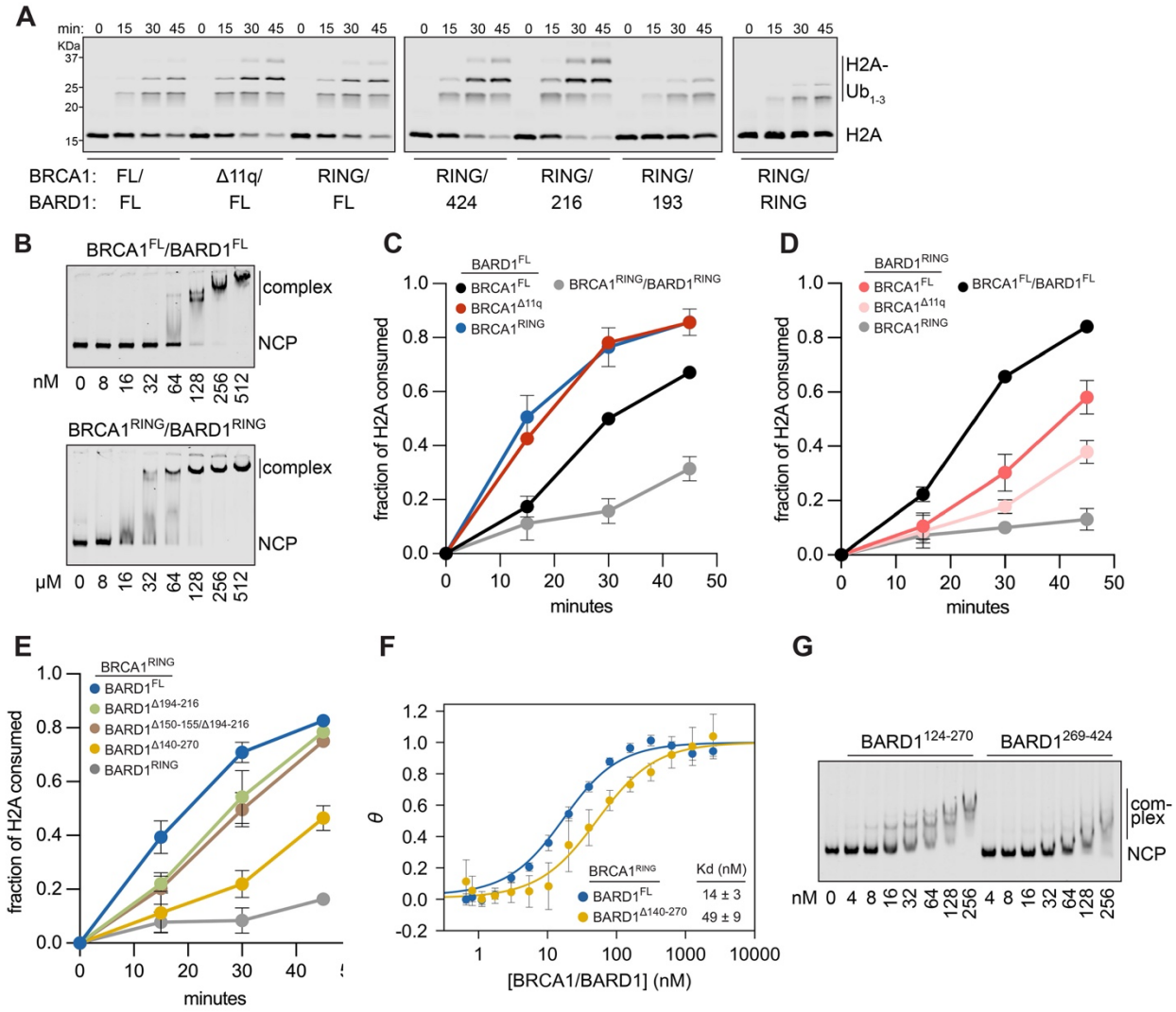

Figure 1—figure supplement 1. Characterization of BRCA1/BARD1 constructs. (A) Representative time-course nucleosome ubiquitylation assays monitoring H2A-Ub efficiency of different BRCA1/BARD1 constructs quantified in Panel E and Figure 1B. These data are representative of the basic assay set-up for other time-course H2A-Ub assays in this study. **(B)** Electrophoretic mobility shift assay (EMSA) comparing the nucleosome binding of full-length BRCA1/BARD1 (top) to the minimal RING heterodimer (bottom). Data shown are representative of n=2 independent experiments. **(C-E)** Quantification of H2A-Ub assays using the indicated BRCA1/BARD1 constructs. Data show the mean; error bars are ± 1-s.d. of n=3 independent experiments. **(F)** Comparison of nucleosome binding affinity from fluorescence-quenching based measurements using the indicated BRCA1/BARD1 constructs. Data show the mean; error bars are ± 1-s.d. of n=4 independent experiments. **(G)** EMSA monitoring nucleosome binding by the indicated BARD1 IDR fragments. Data shown are representative of n=2 independent experiments.

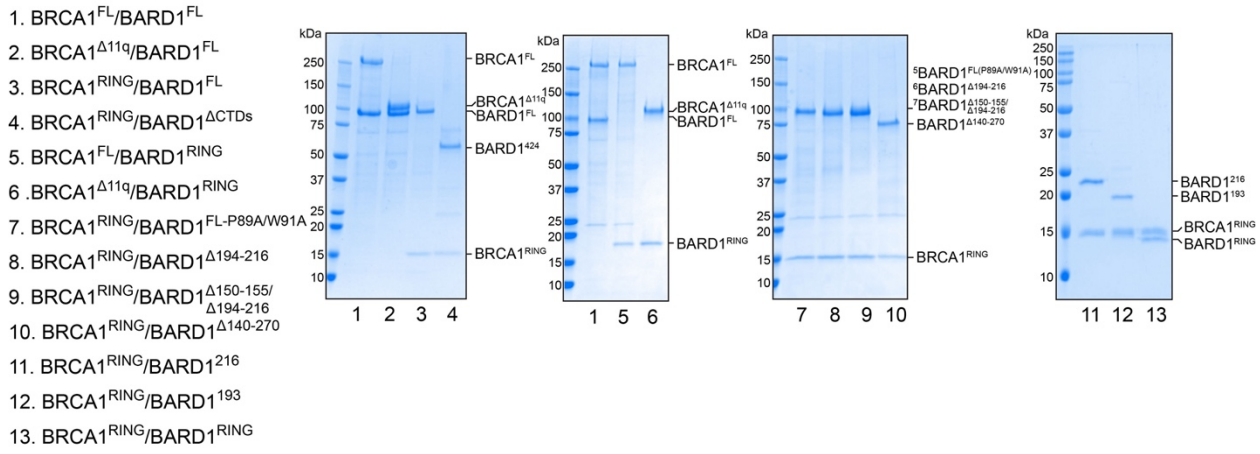

Figure 1—figure supplement 2. Coomassie-stained SDS-PAGE gels of BRCA1/BARD1 constructs used in this study.

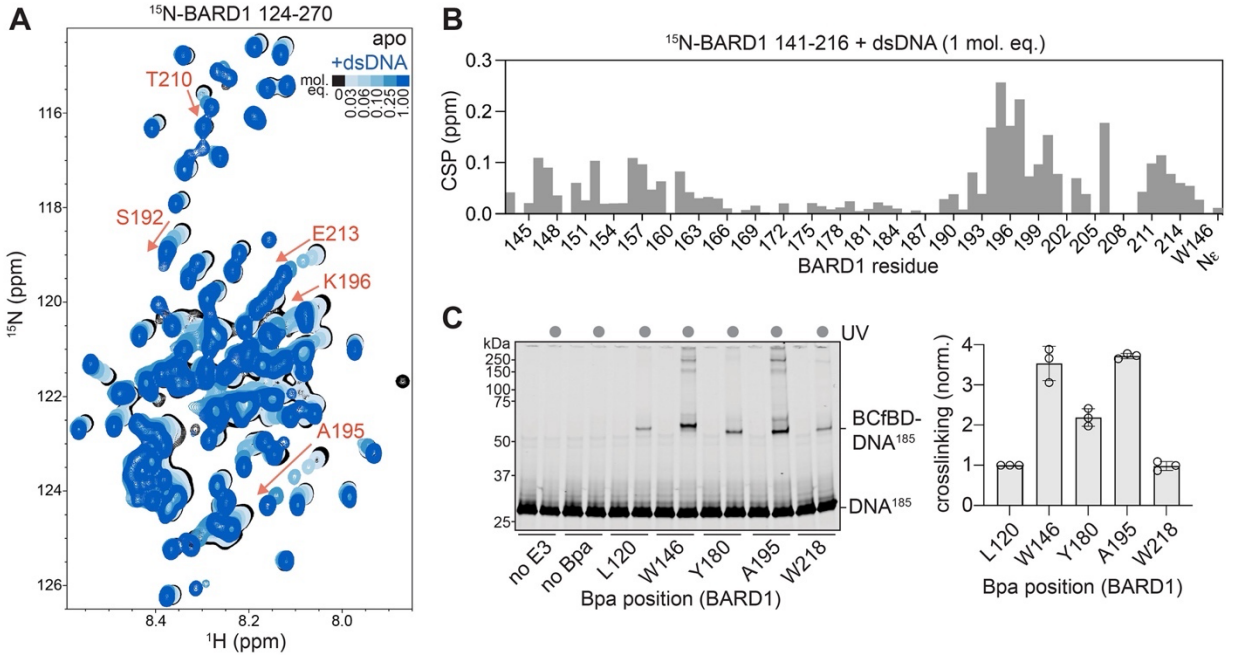

Figure 2. The BARD1 IDR binds to nucleosomes via DNA. (A) $^{1}H^{15}N$-HSQC NMR titration spectra of ^{15}N-BARD1 124-270 with a 36-bp dsDNA fragment. Darker shades of blue correspond to increasing amounts of DNA added. A subset of highly affected signals is labelled with their residue identities, with arrows showing their trajectories over the course of the titration. **(B)** $^{1}H^{15}N$-HSQC NMR amide chemical shift perturbations (CSPs) observed to ^{15}N-BARD1 141-216 signals when bound to a 36-bp dsDNA fragment (1:1 molar equivalent complex). **(C)** Representative SDS-PAGE gel monitoring in-gel fluorescence (labelled DNA) of UV-induced Bpa crosslinking of BRCA1-f-BARD1^{221} to nucleosomes (left). Quantification of Bpa crosslinking experiments with nucleosomes (right). The intensity of each crosslinked band was normalized to the intensity of the L120Bpa crosslinked band for each replicate experiment. Graph bars show the mean; error bars are ± 1-s.d. and the open circles are the values of individual replicates for of n=3 independent experiments.

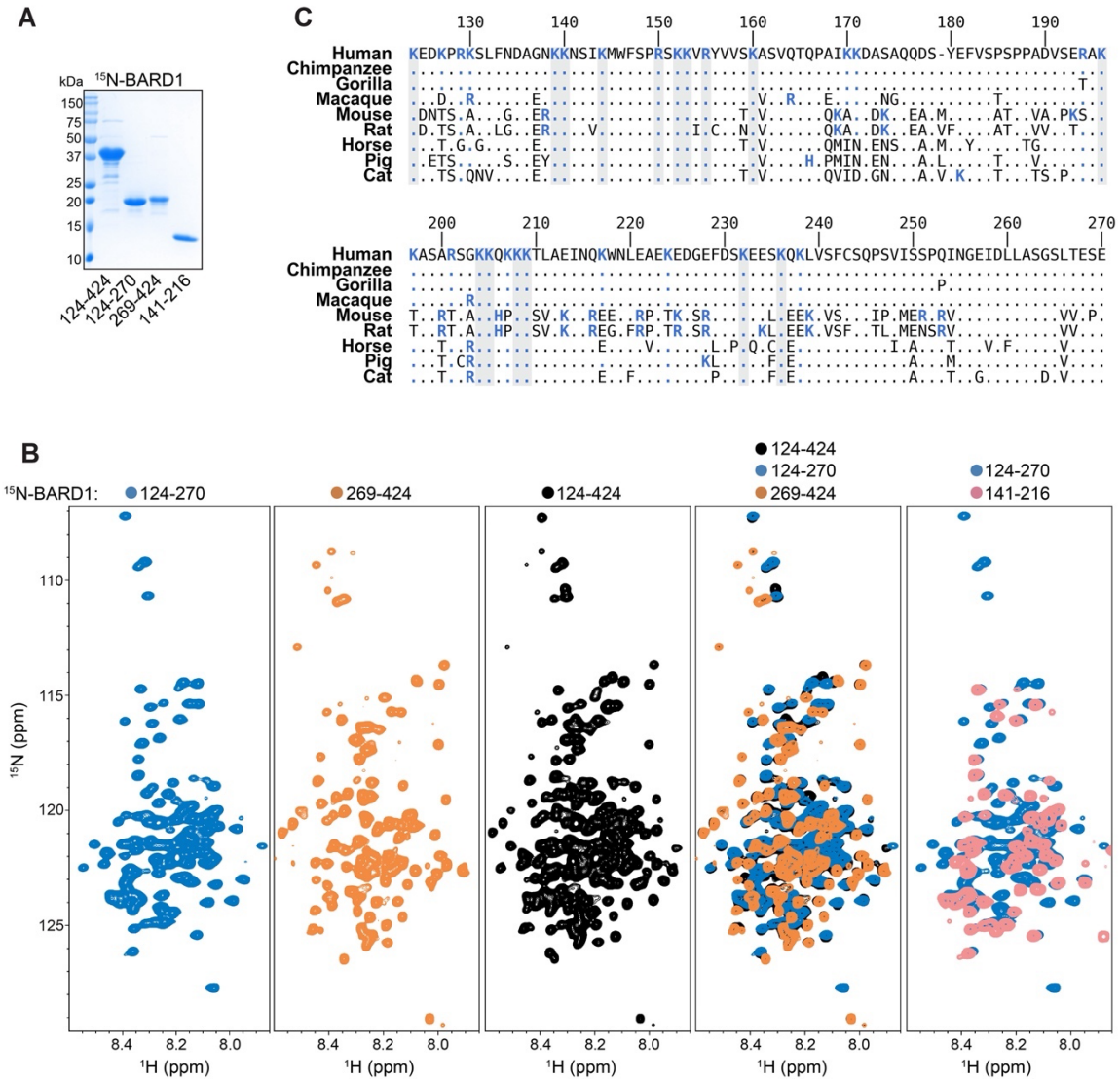

Figure 2—figure supplement 1. Characterization of the BARD1 intrinsically disordered region. (A) Coomassie-stained SDS-PAGE gel of BARD1 fragments used in NMR experiments. **(B)** $^{1}H^{15}N$-HSQC NMR spectra of the indicated ^{15}N-labelled BARD1 fragments. **(C)** Multiple-sequence alignment of BARD1 124-270 with a representative subset of homologs. Residue identities that are conserved to the human sequence are indicated by the presence of a period in place of a residue letter. Basic residues (Lys, Arg, His) are color coded in blue, and basic positions that are fully conserved across all species are highlighted with a gray background.

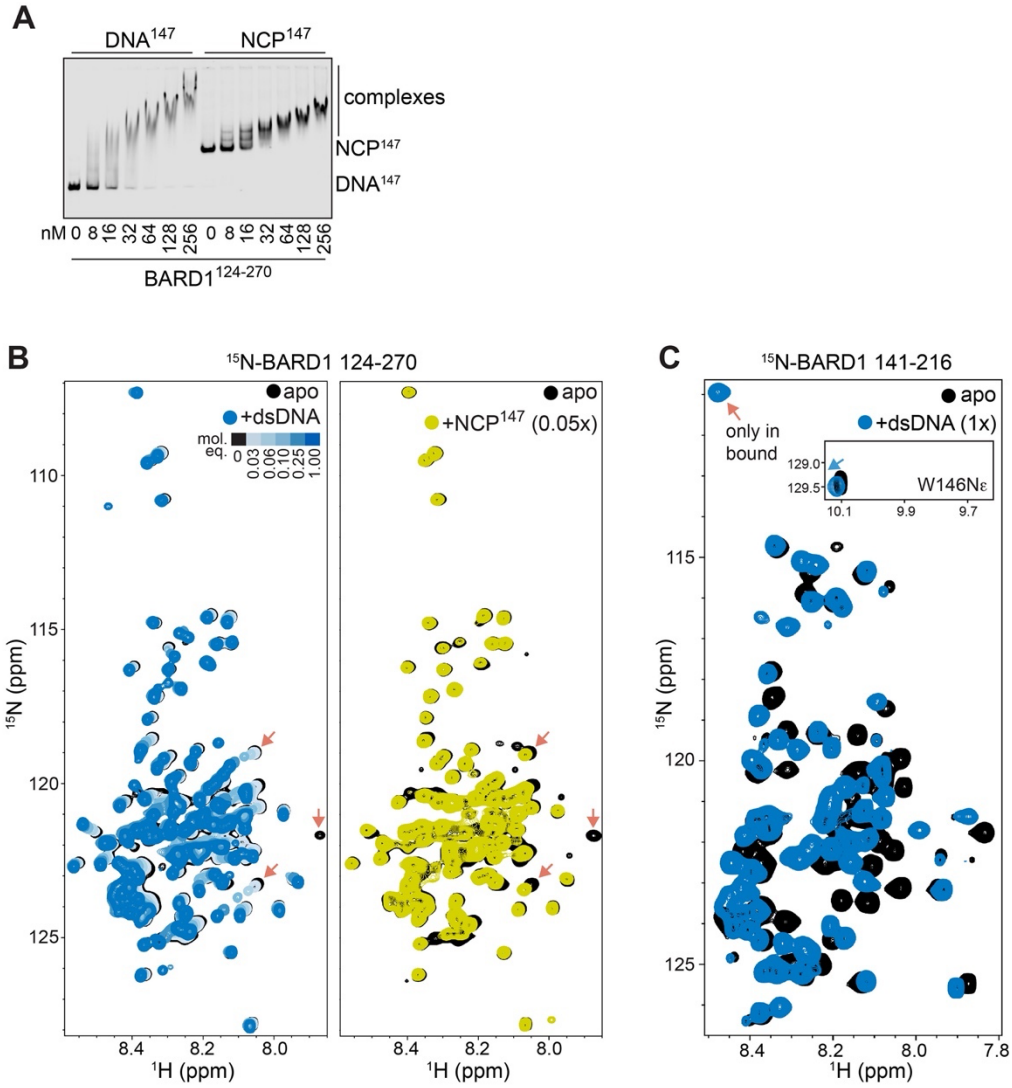

Figure 2—figure supplement 2. NMR analysis of BARD1 IDR-DNA and IDR-nucleosome complexes. (A) EMSA comparing DNA and nucleosome binding by BARD1 124-270. Data shown are representative of n=2 independent experiments. **(B)** $^{1}H^{15}N$-HSQC NMR spectra of ^{15}N-BARD1 124-270, titrating a 36-bp dsDNA fragment (left), and a single titration point with nucleosomes (right). The red arrows point to signals that are similarly affected between the dsDNA- and nucleosome-bound samples. **(C)** $^{1}H^{15}N$-HSQC NMR spectra of ^{15}N-BARD1 141-216 with a 36-mer dsDNA fragment. Data from panel C are also shown in Figure 4—figure supplement 3A.

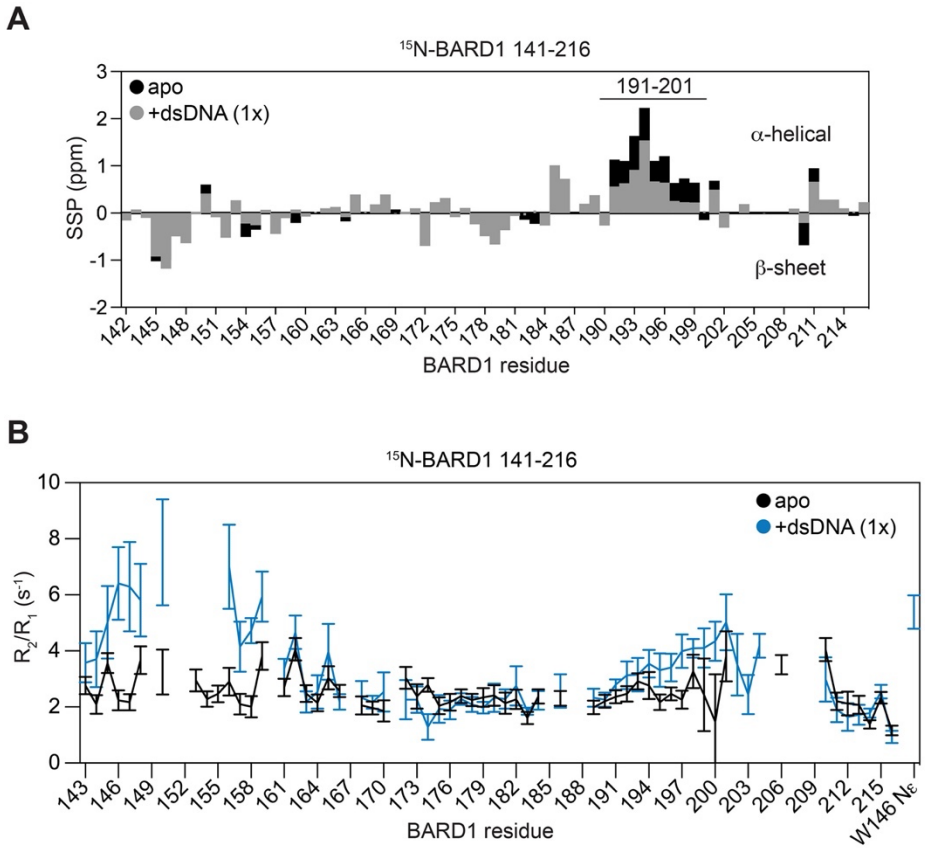

Figure 2—figure supplement 3. Changes in dynamics and secondary structure of the BARD1 IDR bound to DNA. (A) Changes in secondary structural propensity (SSP) of ^{15}N-BARD1 141-216 when bound to a 36-bp dsDNA fragment. The black bars for apo BARD1 are behind the gray bars where DNA was added. **(B)** T1/T2 dynamics measurements for amide signals of ^{15}N-BARD1 141-216 in apo form and bound to dsDNA (1:1 molar equivalent complex). Data from panel B are also shown in Figure 4—figure supplement 3C.

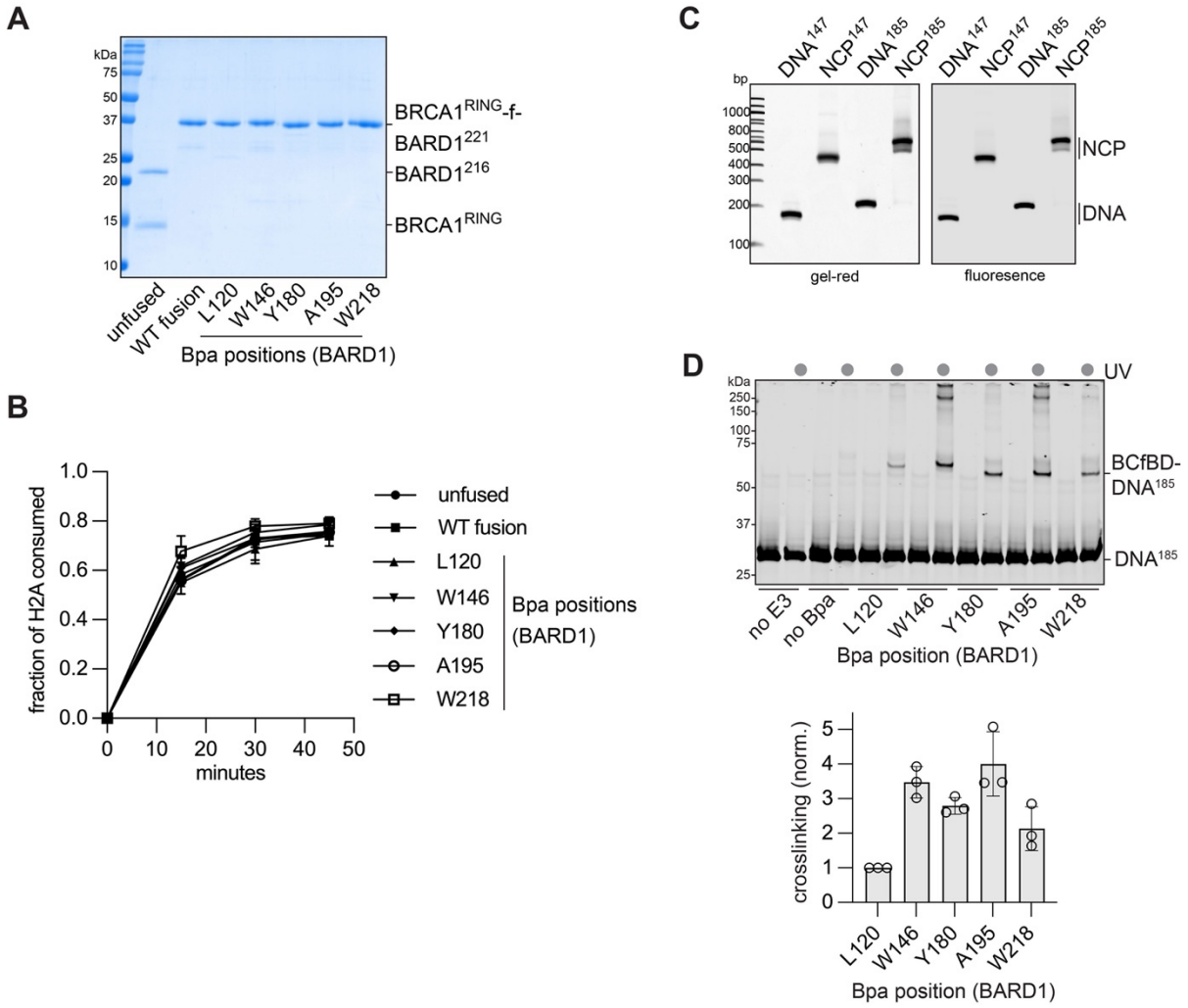

Figure 2—figure supplement 4. UV-induced Bpa crosslinking of BRCA1/BARD1 to nucleosomal DNA. (A) Coomassie-stained SDS-PAGE gel of unfused BRCA1^{RING}/BARD1^{216} heterodimers and BRCA1-f-BARD1^{221} constructs with and without Bpa incorporation. **(B)** H2A-Ub activity of unfused heterodimers compared to wild-type and Bpa-incorporated BRCA1-f-BARD1^{221}. Data show the mean; error bars are ± 1-s.d. of n=3 independent experiments. **(C)** Native gel of fluorescently labelled DNA and nucleosomes used in Bpa crosslinking experiments. **(D)** Representative data of in-gel fluorescence signal from of a UV-induced crosslinking reaction to free 185-bp '601' DNA (DNA^{185}, top) and quantification of crosslinking experiments (bottom). The intensity of each crosslinked band was normalized to the L120Bpa crosslinked band intensity for each replicate experiment. Data bars show the mean; error bars are ± 1-s.d. and the open circles are the values of individual replicates for of n=3 independent experiments.

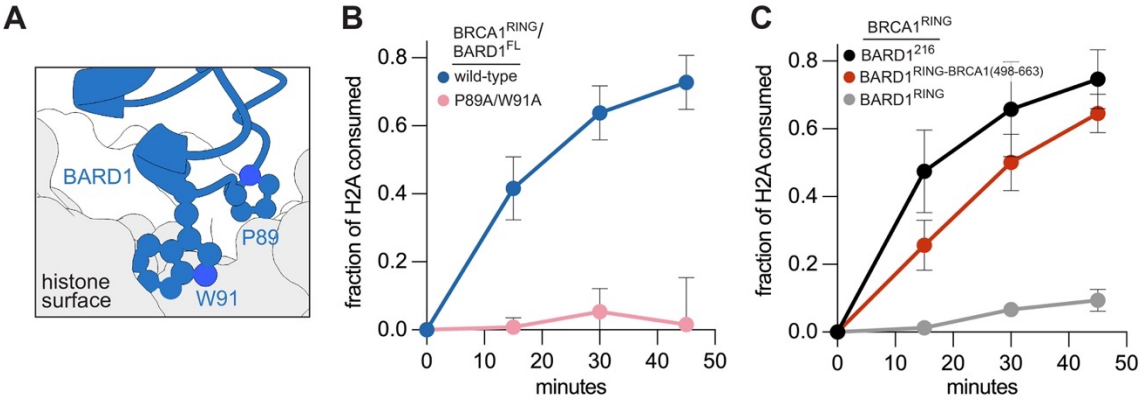

Figure 3. Contribution of BARD1 DNA-binding and RING-histone binding to H2A-Ub activity. (A) The BARD1 RING-histone interface showing the locations of BARD1 P89 and W91 relative to the histone surface (PDB: 7JZV). **(B, C)** Quantification of time-course H2A-Ub assays using the indicated BRCA1/BARD1 constructs. Data show the mean; error bars are ± 1-s.d. of n=3 independent experiments. Two single time-points were determined to be outliers in panel C and excluded from analysis. Values for these excluded points are included as source data.

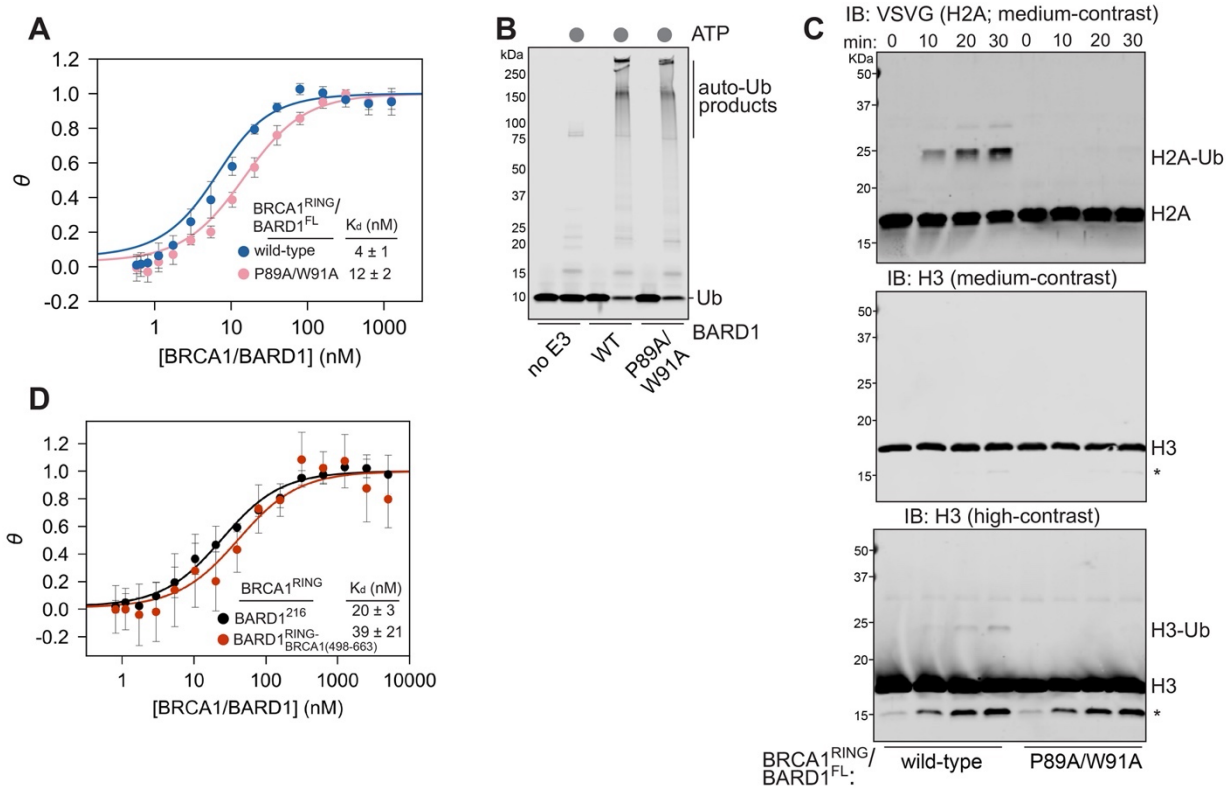

Figure 3—figure supplement 1. Nucleosome binding and Ub ligase activity of BARD1 RING mutants and DNA-binding chimeric constructs. (A) Comparison of nucleosome binding affinity using the indicated BRCA1/BARD1 constructs. Data show the mean; error bars are ± 1-s.d. of n=3 independent experiments. **(B)** Auto-ubiquitylation assay using $BRCA1^{RING}/BARD1^{FL}$ (wild-type or P89A/W91A). The assay monitors depletion of Ub and appearance of high molecular weight auto-Ub products in the presence of BRCA1/BARD1. Data shown is representative of n=2 independent experiments. **(C)** Nucleosome ubiquitylation assay using the indicated BRCA1/BARD1 constructs and blotting for VSVG-tagged H2A (top) and H3 (middle and bottom). The asterisk denotes a proteolysis product of H3 that appears over the time-course. **(D)** Comparison of nucleosome binding affinity using the indicated BRCA1/BARD1 constructs. Data show the mean; error bars are ± 1-s.d. of n=2 independent experiments.

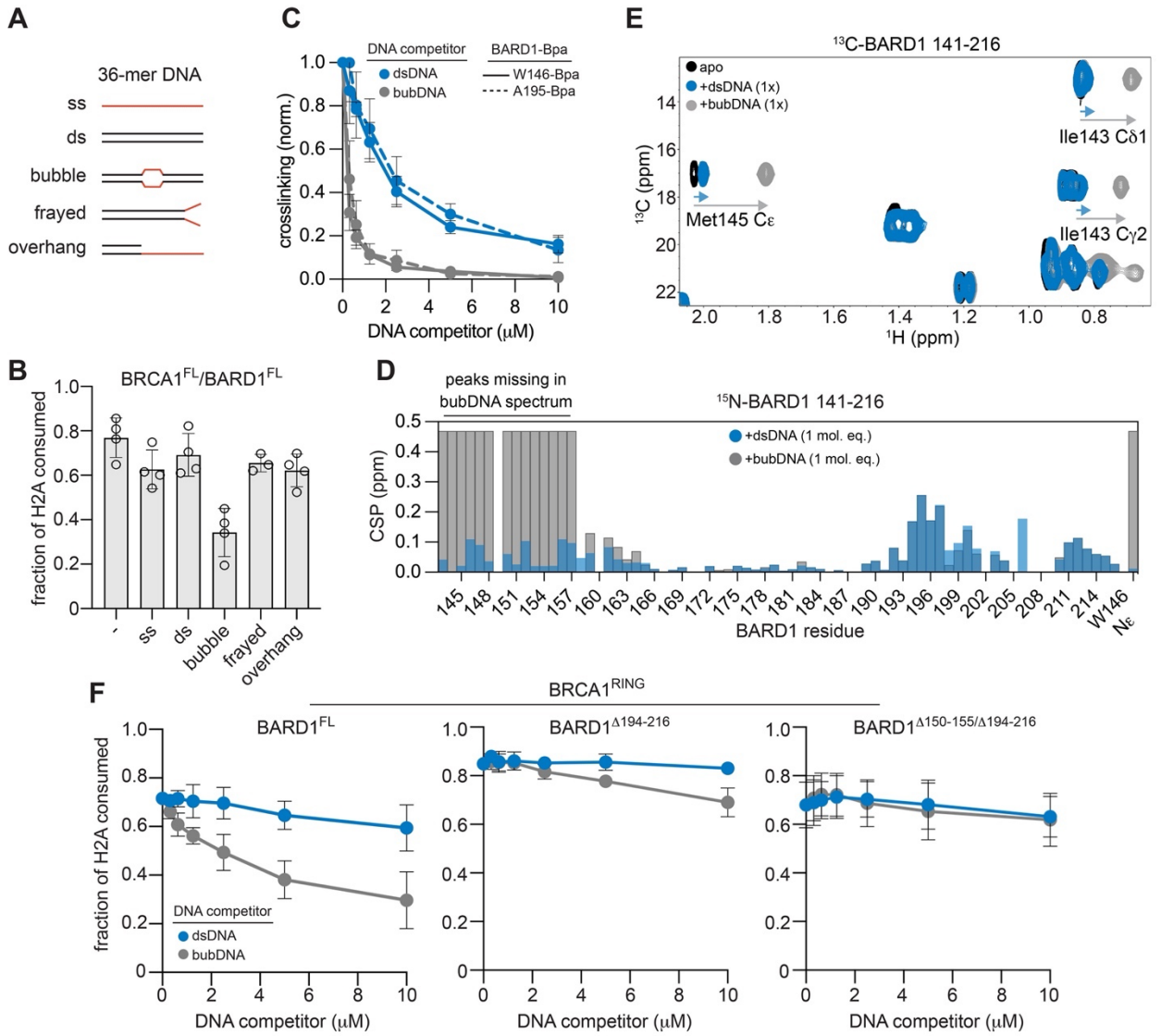

Figure 4. Inhibition of nucleosome binding and H2A-Ub by specialized DNA structures. **(A)** Design of 36-mer DNA competitor fragments used in H2A-Ub activity, Bpa crosslinking, and NMR assays. Red indicates non-base-paired regions. The number of unpaired bases or base-pairs is: ss – 36; ds – 0; bubble – 8; frayed – 8; ssOverhang – 24. **(B)** Single time-point H2A-Ub inhibition assays using $BRCA1^{FL}/BARD1^{FL}$ (100 nM) and the indicated competitor DNA (2.5 μM). Data show the mean; error bars are ± 1-s.d.; and open circles are individual data points of n=4 independent experiments. One outlier point for "frayed-DNA" was excluded from the analysis. **(C)** Inhibition of UV-induced Bpa crosslinking between the indicated BRCA1-f-$BARD1^{221}$ Bpa-incorporated constructs and NCP^{185} substrates in the presence of increasing amounts of dsDNA or bubble-DNA competitor. Data show the mean; error bars are ± 1-s.d. of n=3 (W146Bpa) or n=4 (A195Bpa) independent experiments. **(D)** $^{1}H^{15}N$-HSQC NMR CSPs observed to ^{15}N-BARD1 141-216 signals when bound to a 36-mer dsDNA (blue, front) or bubble-DNA (gray, back) fragment (1:1 molar equivalent complex). Signals for residues 143-157 are broadened beyond detection in the bubble-DNA-bound spectrum, and gray bars are equal to the CSP value for the W146Ne CSP that was observed (see Extended Data Figure 3c, d for spectra). **(E)** Selected region of ^{13}C-HSQC spectra of ^{13}C-BARD1 141-216 in 1:1 molar equivalent complex with

1060 dsDNA fragment or bubble-DNA fragment. Signal trajectories in bound spectra are indicated by
1061 arrows. **(F)** Single time-point H2A-Ub inhibition assays using heterodimers containing
1062 $BRCA1^{RING}/BARD1^{FL}$ (left, 12 min endpoint) or the indicated BARD1 internal deletion mutant
1063 (middle and right, 20 min endpoint) and increasing amounts of dsDNA or bubble-DNA
1064 competitor. The same amount of E3 (50 nM) was used for each BRCA1/BARD1 truncation.
1065 Data show the mean; error bars are ± 1-s.d. of n=3 independent experiments. One time-point
1066 from Panels B and C each were determined to be outliers and excluded from analysis. Values
1067 for these points are included as source data.
1068
1069
1070
1071
1072
1073
1074
1075
1076
1077
1078
1079
1080

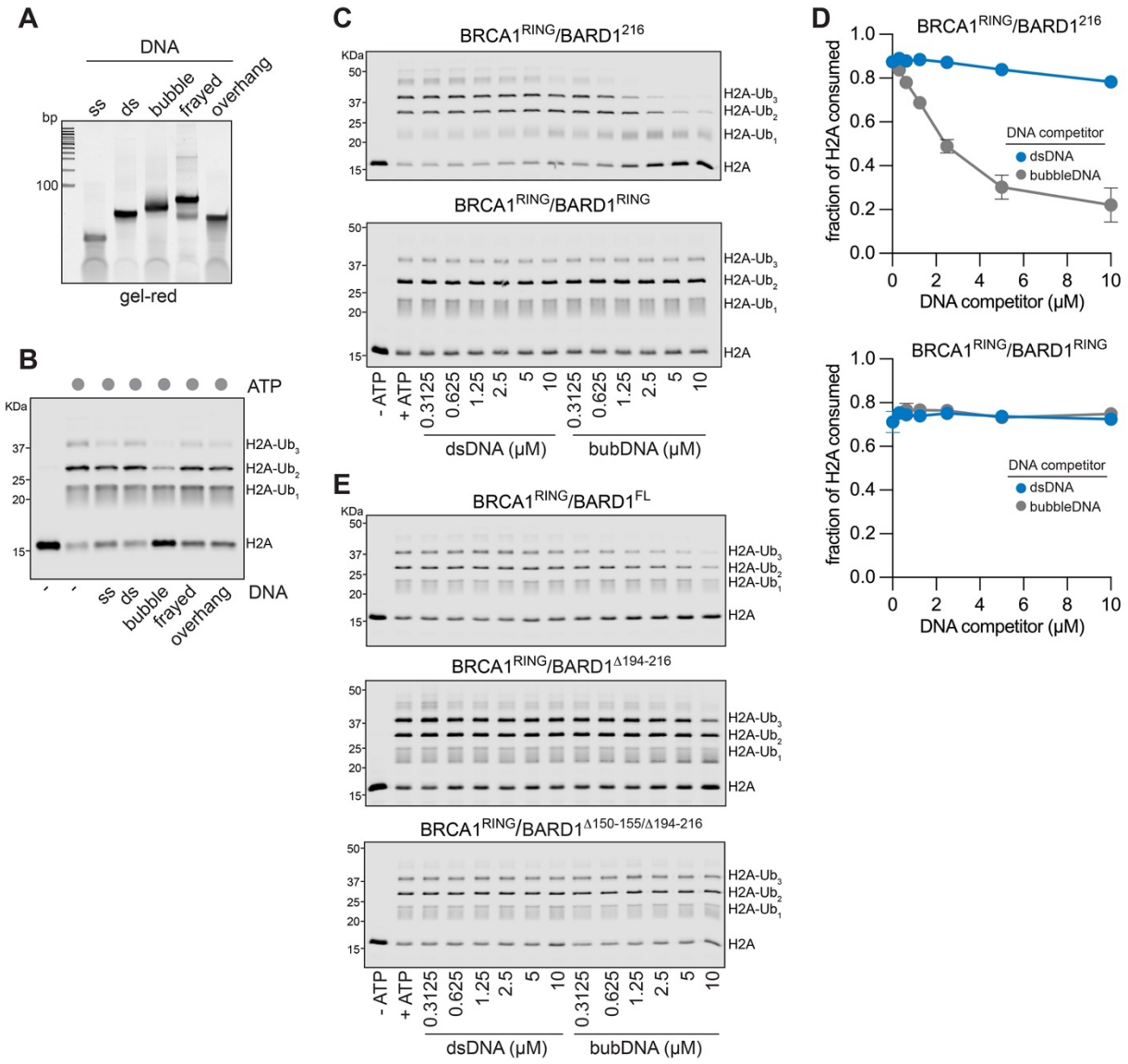

Figure 4—figure supplement 1. Assembly of competitor DNA fragments and inhibition of H2A-Ub activity. (A) DNA-stained native-gel of annealed DNA competitor fragments. Amounts loaded were normalized to show similar band-intensity for each fragment. **(B)** Representative gel data of H2A-Ub inhibition assay using full-length BRCA1/BARD1 (100 nM) and the indicated DNA competitor fragment (2.5 mM) **(C)** Representative gel data of single time-point (20 min) H2A-Ub inhibition assays using $BRCA1^{RING}/BARD1^{216}$ (top, 50 nM E3) and $BRCA1^{RING}/BARD1^{140}$ (bottom, 750 nM E3) and indicated amounts of dsDNA and bubble-DNA competitors. **(D)** Quantification of H2A-Ub DNA-competitor inhibition assays from panel b using the indicated BRCA1/BARD1 constructs. Data show the mean; error bars are ± 1-s.d. of n=3 independent experiments. **(E)** Representative gel data of single time-point H2A-Ub inhibition assays using $BRCA1^{RING}/BARD1^{FL}$ (top, 50 nM E3, 12 min endpoint), $BRCA1^{RING}/BARD1^{\Delta 194-216}$ (middle, 50 nM E3, 20 min endpoint), and $BRCA1^{RING}/BARD1^{\Delta 150-155/\Delta 194-216}$ (bottom, 50 nM E3, 20 min endpoint) and indicated amounts of dsDNA and bubble-DNA competitors.

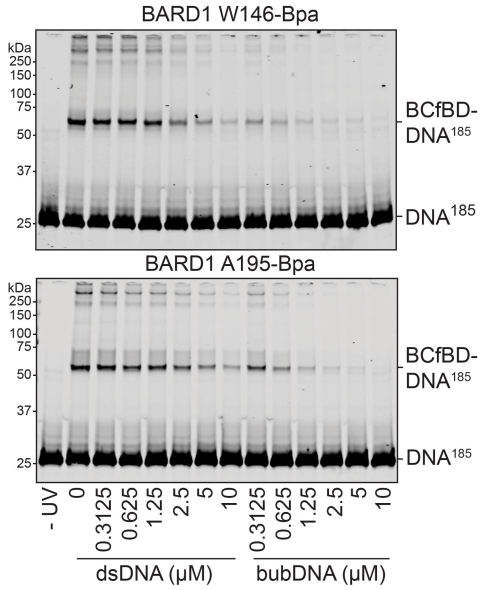

Figure 4—figure supplement 2. Inhibition of UV-induced Bpa crosslinking of BRCA1/BARD1 to nucleosomal DNA. Representative data of in-gel fluorescence signal from a UV-induced Bpa crosslinking reaction between W146Bpa (top) and A195Bpa (bottom) BRCA1-f-BARD1^{221} to 185-bp '601' nucleosomes (NCP^{185}) in the presence of dsDNA and bubble-DNA competitors. Quantified data from n=3 replicate experiments are shown in Figure 4C.

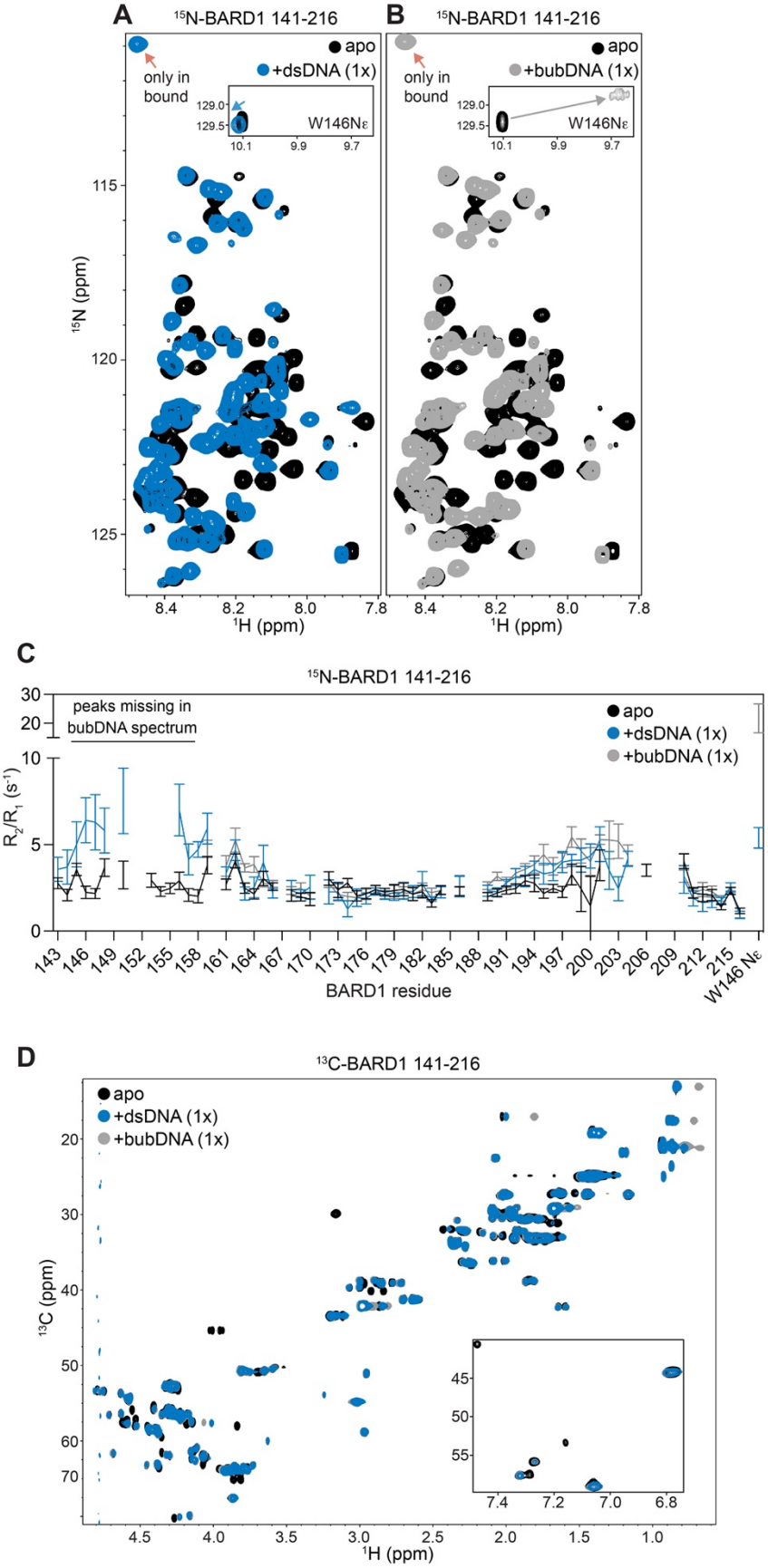
A
15N-BARD1 141-216
apo
+dsDNA (1x)
only in bound
W146Nε
15N (ppm)
1H (ppm)
B
15N-BARD1 141-216
apo
+bubDNA (1x)
only in bound
W146Nε
1H (ppm)
C
15N-BARD1 141-216
peaks missing in bubDNA spectrum
apo
+dsDNA (1x)
+bubDNA (1x)
R2/R1 (s-1)
BARD1 residue
W146 Nε
D
13C-BARD1 141-216
apo
+dsDNA (1x)
+bubDNA (1x)
13C (ppm)
1H (ppm)

1127

Figure 4—figure supplement 3. Comparison of dsDNA and bubble-DNA binding to the BARD1 IDR by NMR. (A) $^{1}H^{15}N$-HSQC NMR spectra of ^{15}N-BARD1 141-216 with a 36-mer dsDNA fragment or **(B)** a 36-mer bubble-DNA fragment with 8-bp of mismatch. Both complexes were assembled at 1:1 molar equivalent. The W146Nε signals are inlaid, and the red arrows point to a signal that is present exclusively in the DNA-bound spectra. **(C)** T1/T2 dynamics measurements for amide signals of ^{15}N-BARD1 141-216 in apo form and bound to dsDNA or bubble-DNA (1:1 molar equivalent complex). **(D)** $^{1}H^{13}C$-HSQC NMR spectra of ^{13}C-BARD1 141-216 with a 36-mer dsDNA fragment (blue), or a 36-mer bubble-DNA fragment with 8-bp of mismatch (gray). Both complexes were assembled at 1:1 molar equivalent. Data from panel A are also shown in Figure 2—figure supplement 2C. A subset of data from panel C (apo and +dsDNA) are also shown in Figure 2—figure supplement 3B.

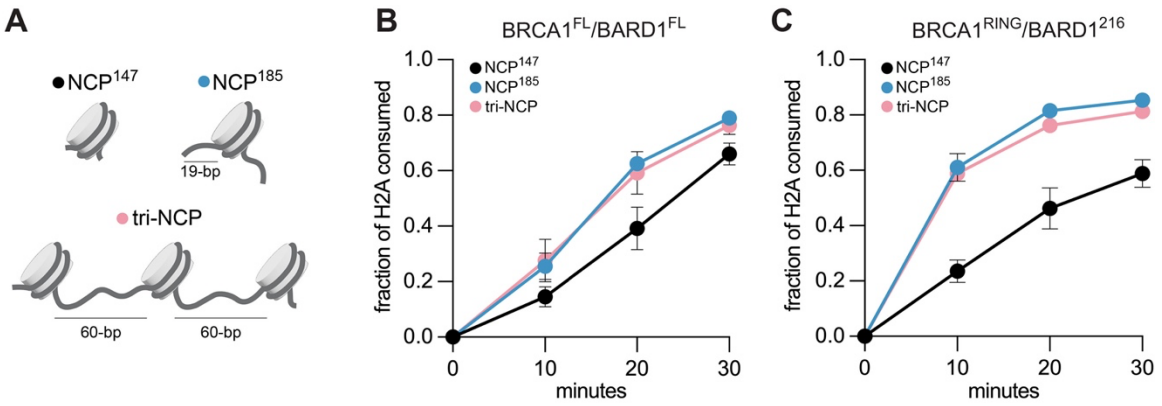

Figure 5. An unmodified mono-nucleosome with linker DNA is an optimal substrate for BRCA1/BARD1. (A) Schematic of chromatin substrates used for H2A-Ub activity and nucleosome binding assays in panels b and c. The length of linker-DNA is indicated next to the NCP^{185} and tri-NCP. **(B, C)** Quantification of time-course H2A-Ub assays using the indicated BRCA1/BARD1 constructs and chromatin substrates. Data show the mean; error bars are ± 1-s.d. of n=3 independent experiments.

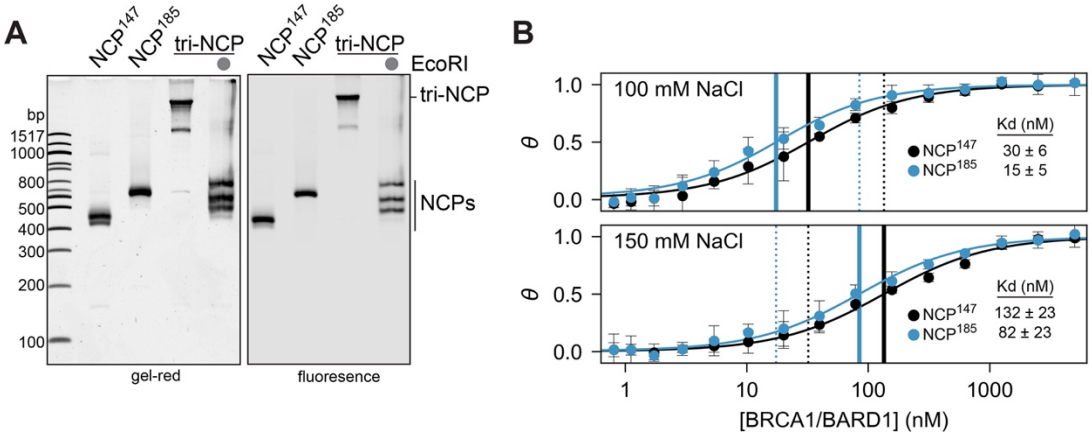

Figure 5—figure supplement 1. Analysis of chromatin substrates (A) DNA-stained (left) and fluorescence (right) native gel of chromatin substrates used for H2A-Ub activity assays in Figure 5b and c. EcoRI digestion of tri-NCPs is used to confirm octamer binding saturation. **(B)** Comparison of nucleosome binding affinity between $BRCA1^{RING}/BARD1^{216}$ and NCP^{147} and NCP^{185} substrates at 100 mM (top) and 150 mM (bottom) buffer-salt concentration (NaCl). The solid vertical lines denote the position of K_d values for the indicated buffer-salt concentration, and the dotted vertical lines denote the position of K_d values from the other buffer-salt concentration. Data show the mean; error bars are ± 1-s.d. of n=3 independent experiments using both NCP^{147} and NCP^{185}, with an additional replicate (total of n=4) for NCP^{147}.

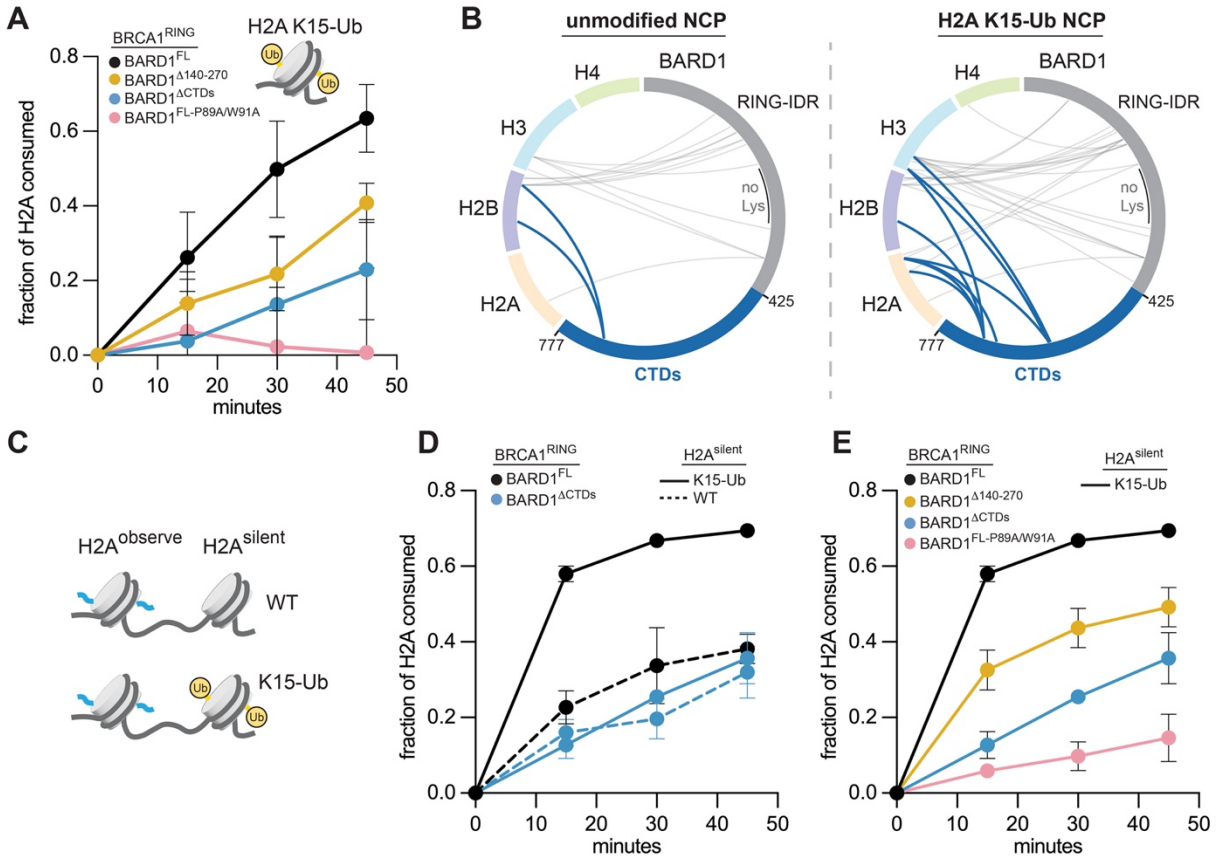

Figure 6. Enhancement of H2A-Ub activity using chromatin substrates with pre-installed H2A K15-Ub. (A) Quantification of time-course H2A-Ub assays using homogenously modified H2A K15-Ub mono-nucleosome substrates and indicated BRCA1/BARD1 constructs. **(B)** Intermolecular crosslinks observed by chemical crosslinking and MS analysis between BARD1 and histones using wild-type (left) and H2A K15-Ub (right) 147-bp '601' nucleosomes and $BRCA1^{RING}/BARD1^{FL}$ heterodimers. Crosslinks to histones emanating from the CTDs of BARD1 are shown in blue, and the RING-IDR region in gray. A lysine-depleted region of the BARD1 IDR is labelled and indicated by a black bar. **(C)** Design of asymmetric di-NCP substrates. **(D, E)** Quantification of time-course H2A-Ub assays using the indicated combinations of di-NCP substrate and BRCA1/BARD1 heterodimer. For panels A, D, and E, data show the mean; error bars are ± 1-s.d. of n=3 independent experiments. One time-point from Panel A was determined to be an outlier and excluded from analysis. The excluded value is reported as source data.

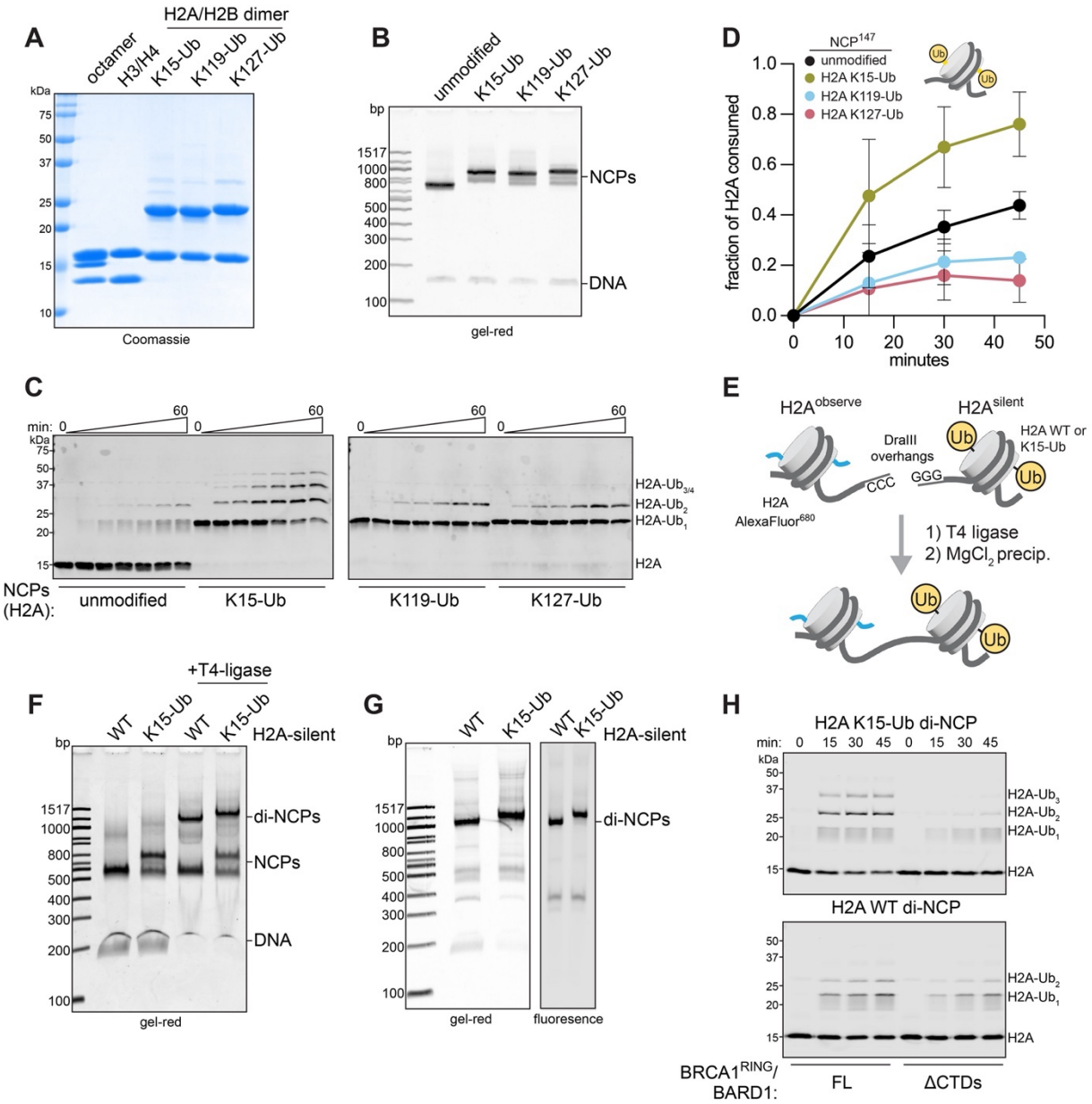

Figure 6—figure supplement 1. Design, assembly, and quality control of H2A K15-Ub chromatin substrates. (A) Coomassie-stained SDS-PAGE gel of wild-type histones and dichloroacetone linked H2A-Ub/H2B dimers. **(B)** DNA-stained native gel of mono-nucleosomes with and without H2A-Ub incorporation at the indicated positions. **(C)** Example data of H2A-Ub activity assay using full-length BRCA1/BARD1 and preinstalled H2A-Ub NCP substrates. Western blots were probed for H2A. **(D)** Quantification of time-course H2A-Ub assays using unmodified or pre-installed H2A-Ub chromatin substrates and $BRCA1^{FL}/BARD1^{FL}$. **(E)** Schematic of asymmetric di-NCP assembly strategy. **(F)** DNA-stained native gel of di-NCP ligation reaction. **(G)** DNA-stained (left) and fluorescence (right) native gels of di-NCP substrates after purification by $MgCl_2$ precipitation. **(H)** Example gel data of H2A-Ub activity assay using di-NCP substrates and indicated BRCA1/BARD1 constructs.

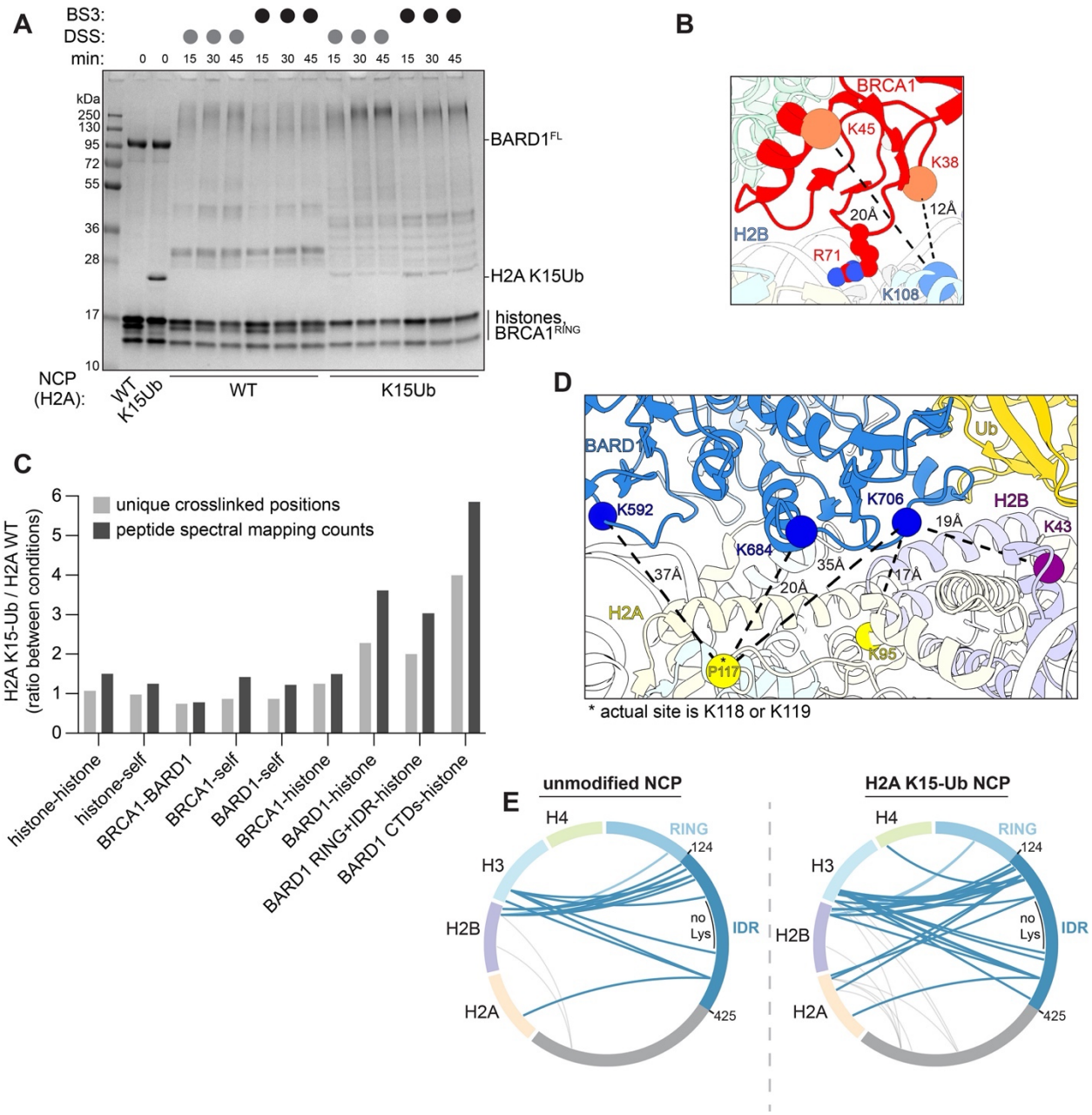

Figure 6—figure supplement 2. Analysis of BRCA1/BARD1 chromatin complexes by chemical crosslinking and mass-spectrometry. (A) Coomassie-stained SDS-PAGE gel of chemical crosslinking reactions used in mass spectrometry analysis **(B)** Crosslinks observed from the RING domain of BRCA1 to ordered regions histones mapped on a high-resolution structure of the complex (PDB: 7JZV). Cα-Cα distances are indicated in the figure. **(C)** Quantitative comparison of crosslinking from reactions with unmodified and H2A K15-Ub NCPs. Different subsets of crosslinks were quantified for the number of unique observed crosslinks and total peptide spectral mapping counts for all crosslinks within a given subset. **(D)** Crosslinks observed from the CTDs of BARD1 to ordered regions histones in the H2A K15-Ub NCP sample mapped on a high-resolution structure (PDB: 7E8I). Cα-Cα distances are indicated. The P117 Cα serves as a proxy for the true crosslinking sites of K118 and K119 that are not modelled, denoted by an asterisk. **(E)** Intermolecular crosslinks observed by chemical crosslinking and MS

analysis between BARD1 and histones using wild-type (left) and H2A K15-Ub (right, separated by dashed line) 147-bp '601' nucleosomes and $BRCA1^{RING}$/$BARD1^{FL}$ heterodimers. Crosslinks to histones emanating from the BARD1 RING-IDR region are highlighted in blue. A lysine-depleted region of the BARD1 IDR is labelled and indicated by a black bar.

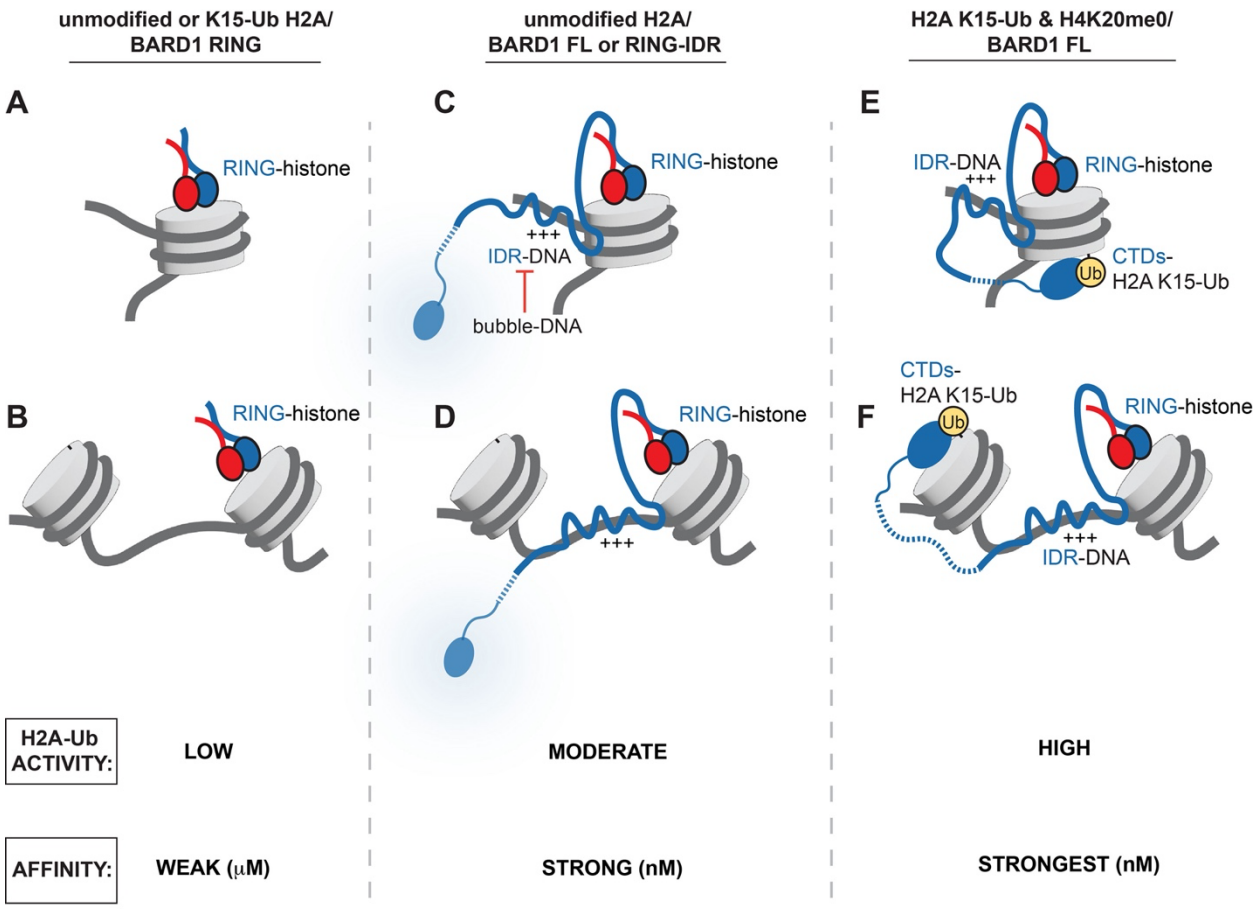

Figure 7. Models of BRCA1/BARD1/chromatin complexes supported by this study. (A, B) Model of the BRCA1/BARD1 minimal RING heterodimer binding to an unmodified mono-nucleosome or higher-order chromatin substrate. **(C, D)** Model of BRCA1/BARD1 (BARD1 full-length or RING-IDR) binding with an unmodified mono-nucleosome or higher-order chromatin substrate. **(E, F)** Model of BRCA1/BARD1^{FL} binding to ubiquitylated chromatin substrates in a 'wrapped complex (panel E) or in a complex that spans nucleosome units (panel F). The relative H2A-Ub activity and affinity of the complexes is indicated below each set of panels.

1300 **Tables**
1301
1302 **Extended Data Table I. Details about BRCA1/BARD1 constructs used in this study.**
1303

Construct	BRCA1 bounds*	BRCA1 tags	BARD1 bounds*	BARD1 tags	Expression system
$BRCA1^{FL}$/ $BARD1^{FL}$	1-1863	N-FLAG	1-777	N-TwinStrepII	*Sf9*
$BRCA1^{\Delta 11q}$/ $BARD1^{FL}$	1-264, 1366-1863	N-FLAG	1-777	N-TwinStrepII	*Sf9*
$BRCA1^{RING}$/ $BARD1^{FL}$	1-112	N-FLAG	1-777	N-TwinStrepII	*Sf9*
$BRCA1^{RING}$/ $BARD1^{\Delta CTDs}$	1-112	N-FLAG	1-424	N-TwinStrepII	*Sf9*
$BRCA1^{FL}$/ $BARD1^{RING}$	1-1863	N-FLAG	1-140	N-TwinStrepII	*Sf9*
$BRCA1^{\Delta 11q}$/ $BARD1^{RING}$	1-264, 1366-1863	N-FLAG	1-140	N-TwinStrepII	*Sf9*
$BRCA1^{RING}$/ $BARD1^{\Delta 194-216}$	1-112	N-FLAG	1-193, 217-777	N-TwinStrepII	*Sf9*
$BRCA1^{RING}$/ $BARD1^{\Delta 150-155/\Delta 194-216}$	1-112	N-FLAG	1-149, 156-193, 217-777	N-TwinStrepII	*Sf9*
$BRCA1^{RING}$/ $BARD1^{\Delta 140-270}$	1-112	N-FLAG	1-139, 271-777	N-TwinStrepII	*Sf9*
$BRCA1^{RING}$/ $BARD1^{216}$	1-110	N-6xHis	26-216	none	*E. coli*
$BRCA1^{RING}$/ $BARD1^{193}$	1-110	N-6xHis	26-193	none	*E. coli*
$BRCA1^{RING}$/ $BARD1^{RING}$	1-110	N-6xHis	26-140	none	*E. coli*

1304
1305 * BRCA1 UniProt sequence ID: P38398-1; BARD1 UniProt sequence ID: Q99728-1
1306
1307
1308
1309
1310
1311
1312
1313

1314 **Methods**

1315 **Protein, nucleosome, and experimental reagent production**

1316 *Ubiquitylation machinery:* Human E1 (UBA1), E2 (UBE2D3), and ubiquitin (wild-type and Q2C
1317 mutant) were expressed and purified as previously described(Brzovic et al., 2003; Christensen
1318 et al., 2007; Lazar et al., 1997). For a full list of BRCA1/BARD1 truncation constructs, their
1319 residue bounds, purification/epitope tags, and expression system, see Extended Data Table I.

1320

1321 *BRCA1/BARD1 from E. coli:* For purification of truncated BRCA1/BARD1 heterodimers from *E.*
1322 *coli* expression ($BRCA1^{RING}/BARD1^{RING}$, $BRCA1^{RING}/BARD1^{193}$, and $BRCA1^{RING}/BARD1^{216}$),
1323 plasmids containing 6xHis-tagged BRCA1 (pCOT7n) and untagged BARD1 (pET28n) were co-
1324 transformed into *E. coli* BL21 (DE3) cells, grown in LB media at 37 °C to OD_{600nm} of 0.6-0.8,
1325 supplemented with 100 μM $ZnCl_2$ and induced with 0.2 mM IPTG for ~16 hours at 16 °C. The
1326 cell pellets were resuspended in 30 mL of Ni^{2+} start buffer (25 mM Tris-HCl pH 7.5, 500 mM
1327 NaCl, 10 mM imidazole) supplemented with DNase, RNase, EDTA-free protease inhibitors
1328 (Roche) and 1 mM PMSF, lysed by French press, centrifuged, and the supernatant was applied
1329 to a 5 mL HisTrap FF crude column (Cytiva). After extensive washing with Ni^{2+} start buffer
1330 containing 10 mM imidazole and 30 mM imidazole, protein was eluted using the same buffer
1331 supplemented with 500 mM imidazole. The $BRCA1^{RING}/BARD1^{RING}$ and $BRCA1^{RING}/BARD1^{193}$
1332 constructs were concentrated and further purified using a 120 mL Superdex 75 column on an
1333 AKTA FPLC system in SEC buffer (25 mM HEPES-NaOH pH 7.5, 150 mM NaCl, 1 mM DTT;
1334 GE Healthcare). For the $BRCA1^{RING}/BARD1^{216}$, HisTrap elutions were dialyzed into ion-
1335 exchange buffer (25 mM Tris-HCl pH 7.5, 250 mM NaCl, 1 mM DTT) and applied to a 5 mL
1336 HiTrap SP HP column (Cytiva) and eluted over a 12 column-volume (CV) gradient (0.25-1 M
1337 NaCl). Peak fractions were concentrated, aliquoted, and flash frozen.

1338

1339 For Bpa crosslinking experiments, 6xHis-BRCA1$^{1-104}$-(GS)$_6$-BARD1$^{26-221}$ was sub-cloned using
1340 Gibson assembly into a pET28n vector. Constructs for Bpa incorporation were generated via
1341 site-directed mutagenesis to install amber stop codons in place of BARD1 L120, W146, Y180,
1342 A195, and W218. Bpa-mutant Pet28n-6xHis-BRCA1$^{1-104}$-(GS)$_6$-BARD1$^{26-221}$ plasmids were co-
1343 transformed with a pEVOL-pBpF plasmid encoding an Bpa aminoacyl tRNA synthetase (gift
1344 from P. Schultz, Addgene #31190) in *E. coli* BL21 (DE3) cells(Chin Jason W. et al., 2002). At
1345 OD_{600nm}=0.4-0.5, cells were shifted from 37 °C to 16 °C and supplemented with 1 mM Bpa
1346 (dissolved in 1M NaOH; Bachem) and 100 µM $ZnCl_2$. After 30 minutes, protein expression was
1347 induced by addition of 0.02% L-arabinose and 0.2 mM IPTG for ~16 hours at 16 °C. Proteins
1348 were purified as described for the BRCA1^{RING}/BARD1^{216} construct. Truncations that did not
1349 incorporate Bpa were separated via the SP column.
1350
1351 *BRCA1/BARD1 from insect cells:* For insect cell expression, truncation and deletion constructs
1352 were derived from full-length BRCA1 (pFastBac-FLAG-BRCA1$^{1-1863}$; gift from W. Zhao, UT
1353 Health Sciences Center at San Antonio) and insect cell codon-optimized full-length BARD1
1354 (pFastBac-Twin-StrepTagII-BARD1$^{1-777}$; gift from A. Deans, Addgene plasmid #137166)(Tan et
1355 al., 2020) using Gibson assembly cloning (NEB). Baculovirus was generated using the Bac-to-
1356 Bac system in suspension culture *Sf9* cells according to the manufacturers protocols
1357 (Invitrogen). For general *Sf9* growth and virus amplification, SF900-II media (ThermoFisher)
1358 was supplemented with 5% FBS (HyClone) and 1x antibiotic-antimycotic (Gibco). For protein
1359 expression, 15 mL of BRCA1- and 15 mL of BARD1-containing P3 baculoviruses were added to
1360 650 mL of *Sf9* cells at ~1.5x10^6 cells/mL in SF900-II media supplemented with 1% FBS and 1x
1361 antibiotic-antimycotic. Protein expression was carried out for 48-72 hours at 27 °C, shaking at
1362 110 RPM. Following expression, cells were spun down at 150 x g for 10 minutes. The pellet was
1363 resuspended in 30 mL of Strep-start buffer (50 mM Tris-HCl pH 8, 10% glycerol, 150 mM NaCl,

1364 1 mM DTT) supplemented with EDTA-free protease inhibitors and 1 mM PMSF and flash-
1365 frozen. Following freeze-thawing in a 37 °C water bath, additional EDTA-free protease inhibitors
1366 and PMSF were added in addition to 2 µL of benzonase (Sigma Aldrich). All subsequent steps
1367 were performed on ice or in a cold room over a short timeframe to prevent proteolysis (<3 hours
1368 total). Lysis was performed by sonication using a Branson Sonifier 250 (VWR Scientific) by
1369 applying 2 rounds of 15 pulses at 70% duty on power level 8, ensuring that the cell mixture
1370 stayed cold. PMSF was added throughout the lysis protocol. The lysed cells were centrifuged at
1371 41,000 x g for 15 minutes, filtered through a 0.45 mM low protein-binding PVDF filter (Millipore)
1372 and applied to a 1 mL StrepTrap HP column pre-equilibrated in Strep-start buffer (Cytiva). The
1373 column was washed with 8 mL Strep-start buffer supplemented with protease inhibitors, 8 mL
1374 wash buffer (25 mM Tris-HCl pH 7.5, 300 mM NaCl, 0.01% Igepal-CA630, 1 mM DTT, 5 mM
1375 MgCl2, 2 mM ATP, 10% glycerol, EDTA-free protease inhibitors), and an additional 5 mL of
1376 Strep-start buffer. The column was eluted using 6 mL of Strep-start buffer supplemented with 3
1377 mM d-Desthiobiotin (Sigma). The elution was diluted with 20 mL of ion-exchange buffer (25 mM
1378 HEPES-NaOH pH 7.5, 10% glycerol, 1 mM DTT) and applied to a 1 mL SP HP column pre-
1379 equilibrated in ion-exchange buffer containing 75 mM NaCl. The SP column was eluted over 12-
1380 CV (75-500 mM NaCl). Peak fractions were combined and concentrated using a 30K MWCO
1381 concentrator (Amicon), and flash-frozen in small aliquots. Concentrations were estimated by
1382 measuring absorbance at 280 nM using molar extinction coefficients obtained from ProtParam
1383 (Expasy). Concentration estimates were verified by SDS-PAGE and Coomassie staining, and
1384 slight adjustments in concentration were applied to best equalize the amounts of E3 in activity
1385 and binding assays.
1386
1387 *BARD1 intrinsically disordered region:* BARD1 124-270, 141-216, 269-424, and 124-424 were
1388 sub-cloned from pFastBac-6xHis-BARD1$^{1-777}$ (gift from W. Zhao, UTHCSCA) into a modified
1389 pET28 vector containing an N-terminal 6xHis-SUMO tag using Gibson assembly cloning.

1390 Plasmids were transformed into BL21 (DE3) *E. coli*, grown at 37 °C in M9 media supplemented
1391 with appropriate combination of isotopes (^{15}N-NH_4Cl, ^{13}C-glucose; Cambridge Isotopes) to an
1392 OD_{600nm} of 0.6-0.8, and induced with 0.2 mM IPTG for ~16 hours at 16 °C. HisTrap Ni^{2+}
1393 purification was performed as described above for BRCA1/BARD1 constructs expressed in *E.*
1394 *coli*. Elutions were dialyzed into ion exchange buffer (25 mM Tris pH 8.0, 200 mM NaCl, 0.5 mM
1395 EDTA, 1 mM DTT) in the presence of GST-SENP1 (produced in-house) to cleave the SUMO
1396 tag, leaving a non-native serine residue preceding the N-terminus except in the case of 269-
1397 424. The cleaved product was applied at a HiTrap Q column preceding a HiTrap SP column in-
1398 tandem to capture the non-specifically bound DNA (Cytiva). After application, the Q column was
1399 removed, and the SP column was eluted using a 12-CV gradient (0.2-1M NaCl). The peak
1400 fractions were combined, concentrated, and further purified using a Superdex 75 column
1401 equilibrated in NMR buffer (25 mM MOPS-NaOH pH 7.0, 100 mM NaCl, 1 mM EDTA, 0.5 mM
1402 TCEP (tris(2- carboxyethyl)phosphine)).
1403
1404 *Histone purification*: Wild-type and mutant human histones were transformed in *E. coli* BL21
1405 (DE3) *pLysS* cells, grown at 37 °C to an OD_{600nm} of 0.5-0.6, and induced with 0.5 mM IPTG for 2
1406 hours (H4) or 3 hours (H2A-2A, H2B-1K, H3.2) at 37 °C. Histone octamers used for
1407 fluorescence labeling were purified using the one-pot refolding protocol as described previously
1408 using 6xHis-TEV-H2A(Lee et al., 2015; Witus, Burrell, et al., 2021). For nucleosome
1409 ubiquitylation assays, a glycine within the TEV cleavage scar was mutated to a cysteine for
1410 fluorophore conjugation (H2A G-1C) via site-directed mutagenesis. For fluorescence based
1411 binding assays, a cysteine was introduced at H2B D51 via site-directed mutagenesis.
1412
1413 For reconstituting chemically modified H2A-Ub nucleosomes, histones were purified individually
1414 essentially as described(Luger et al., 1999). Briefly, inclusion bodies from 6-8L of histone

1415 expression in LB media were lysed in buffer T (50 mM Tris-HCl pH 7.4, 1 mM EDTA, 100 mM
1416 NaCl), washed by sonication twice in buffer TW (50 mM Tris-HCl pH 7.4, 1 mM EDTA, 100 mM
1417 NaCl, 1% v/v Triton-X100), and then twice again in buffer T. Inclusion bodies were softened by
1418 stirring with a small volume of DMSO (2-3 mL), and extracted with 60 mL of extraction buffer (25
1419 mM Tris-HCl pH 7.5, 7 M guanidinium-HCl, 0.5 mM EDTA, 10 mM DTT). After centrifugation,
1420 the supernatant was dialyzed overnight into ion-exchange buffer (25 mM Tris-HCl pH 7.5, 7 M
1421 deionized urea, 100 mM NaCl, 0.5 mM EDTA, 10 mM DTT), and applied to 2x5 mL HiTrap Q
1422 columns preceding 2x5 mL HiTrap SP columns in-tandem to capture the non-specifically bound
1423 DNA (Cytiva). After sample application, the Q columns were removed, and the SP columns
1424 were eluted using a 12-CV salt gradient (0.1-1M NaCl for H2A and H2B, 0.2-1M NaCl for H3
1425 and H4). The peak fractions were assessed by Coomassie stained SDS-PAGE gel and
1426 Abs_{260}/Abs_{280} value, and the purest fractions were extensively dialyzed into water, aliquoted,
1427 flash frozen, and lyophilized. Lyophilized histones were reconstituted into H2A/H2B dimers,
1428 H3/H4 tetramers, and octamers as previously described(Dyer et al., 2003), and purified via SEC
1429 using Superdex 75 (H2A/H2B) or Superdex 200 (H3/H4 and octamers) columns in SEC buffer
1430 (25 mM Tris-HCl pH 7.5, 2M NaCl, 1 mM DTT).
1431
1432 *Fluorophore conjugation to histones and ubiquitin*: For fluorophore conjugation, Alexa Fluor 680
1433 C_2 maleimide (ThermoFisher), IRDye 680LT maleimide (Li-Cor), and Oregon green 488
1434 maleimide (AAT Bioquest) were reconstituted in DMSO to 10 mM. Fluorophore maleimides
1435 were mixed with octamers containing single cysteine mutants H2A G-1C for H2A-Ub activity
1436 assays (with Alexa Fluor 680 C_2 maleimide or IRDye 680LT maleimide) or H2B D51C for
1437 binding assays (with Oregon green 488 maleimide). Conjugation reactions were performed
1438 using 20 μM octamer and 100 μM fluorophore overnight at 4 °C in conjugation buffer (25 mM
1439 Tris-HCl pH 7.5, 2M NaCl, 1 mM EDTA, 0.5 mM TCEP), and stopped by addition of 10 mM DTT
1440 and flash frozen. Excess fluorophore was removed after nucleosome reconstitution by SEC

1441 using a Superdex 200 increase 10/300 GL column or extensive buffer exchange in a 30K
1442 MWCO concentrator (Amicon). Typical labelling efficiency was ~70%. For labelling of Ub Q2C,
1443 100 μM Alexa Fluor 680 C_2 maleimide was mixed with ~1 mM of Ub Q2C in buffer (25 mM Tris-
1444 HCl pH 7.5, 1 mM EDTA, 0.5 mM TCEP) at 4 °C overnight. The reaction was quenched with 10
1445 mM DTT, and buffer exchanged into reducing buffer (25 mM Tris-HCl pH 7.5, 1 mM EDTA, 10
1446 mM DTT) in a concentrator to remove unconjugated dye, and stored at -80 °C. The fluorophore
1447 labelling efficiency of Ub was calculated to be ~5%.
1448
1449 *Ubiquitin G76C and dichloroacetone crosslinking of H2A-Ub*: H2A K15C, K119C, and K127C
1450 were generated by site-directed mutagenesis and purified as described above for individual
1451 histones. His-TEV-ubiquitin G76C was a gift from C. Wolberger (Addgene plasmid #75299) and
1452 purified as previously described(Morgan et al., 2019; Morgan Michael T. et al., 2016).
1453 Dichloroacetone crosslinking of Ub G76C to H2A single cysteine mutants was performed as
1454 previously described in detail (Morgan et al., 2019), with the exception that the final product
1455 containing Ub, Ub-Ub dimers, and H2A-Ub was not purified by RP-HPLC to remove
1456 unconjugated Ub. Instead, it was lyophilized, and mixed with a slight excess of H2B in unfolding
1457 buffer (25 mM Tris-HCl pH 7.5, 7 M guanidinium-HCl, 0.5 mM EDTA, 1 mM DTT), refolded into
1458 H2A/H2B dimers in refolding buffer (25 mM Tris-HCl pH 7.5, 2M NaCl, 1 mM DTT), and purified
1459 by SEC using a 24 mL Superdex 75 column (GE Healthcare) to separate the H2A-Ub from Ub
1460 species.
1461
1462 *'601' and MMTV DNA:* For large scale purification of 147-bp '601' (gift from K. Luger, CU
1463 Boulder), 185-bp '601' (gift from S. Tan, Penn State Univ.), MMTV (gift from G. Debelouchina,
1464 (UC San Diego), and NLE-trimer '601' (for tri-NCP; gift from K. Luger) DNA, repeat plasmids
1465 from 8-12L of DH5a cells in LB media were subjected to alkaline lysis, phenol-chloroform

1466 extraction, PEG precipitation, EcoRV digestion (NEB), and ion exchange of the excised
1467 fragment by HiTrap DEAE (147-bp '601', 185-bp '601', and MMTV; Cytiva) or mono-Q (NLE-
1468 trimer '601'; GE Healthcare) according to established protocols(Dyer et al., 2003).
1469
1470 For UV-induced Bpa crosslinking and EMSA experiments, fluorophore labelled '601' DNA was
1471 generated using large-scale PCR with Phusion polymerase (produced in-house) from a pGEM-
1472 3z/601 plasmid containing one copy of '601' DNA (gift from J. Widom, Addgene plasmid
1473 #26656)(Lowary & Widom, 1998) with 5'-IRdye700 labelled forward primers (IDT). Following
1474 PCR, the reactions were purified using a 1 mL mono-Q column equilibrated in ion-exchange
1475 buffer (25 mM Tris-HCl pH 8.0, 200 mM NaCl, 1 mM EDTA) over a 10-CV gradient (0.2-1M
1476 NaCl). Peak fractions containing purified 147- and 185-bp DNA fragments were dialyzed into
1477 storage buffer (10 mM Tris-HCl pH 8.0, 1 mM EDTA), concentrated, and stored at -20 °C. The
1478 primer sequences were as follows: 147-fwd: ctggagaatcccggtgccgagg; 147-rev:
1479 acaggatgtatatatctgacacg; 185-fwd: atccctatacgcggccgccctggagaatcccggtgccgagg
1480 ; 185-rev: atcgctgttcaatacatgcacaggatgtatatatctgacacg.
1481
1482 For generation of DNA fragments with DraIII sticky ends for dinucleosome assembly, large scale
1483 PCR was performed as described for the fluorophore-labelled DNA fragments above. Primer
1484 sequences containing DraIII cut-sites were based off those used by Poepsel *et al*. to make
1485 dinucleosomes with 35-bp of linker DNA(Poepsel et al., 2018). Fragments used to reconstitute
1486 nucleosomes containing fluorophore-labelled H2A nucleosomes ($H2A^{observe}$) were generated
1487 using the "147-fwd" primer (sequence above) and the di-NCP reverse primer sequence
1488 (taggtatcgtatCACGGGGTGagatcgctacaggatgtatatatctgacacg). The fragment for the $H2A^{silent}$
1489 nucleosomes were generated using the "147-rev" and the di-NCP-forward primer sequence
1490 (ctgacttattgaCACCCCGTGatgctcgatactgtcatactggagaatcccggtgccgag). The DraIII sites in the
1491 primers are underlined and uppercase. Following PCR purification by 1 mL mono-Q, DNA

1492 fragments were dialyzed into TE/0.1 buffer (10 mM Tris-HCl, 0.1 mM EDTA) and digested with
1493 DraIII-HF in 1x CutSmart buffer for ~20 hr at 37 °C (NEB). Fragments with DraIII sticky ends
1494 were re-purified by 1 mL mono-Q ion-exchange, dialyzed into storage buffer (10 mM Tris-HCl, 1
1495 mM EDTA), concentrated, and stored at -20 °C.
1496
1497 *Nucleosome reconstitution:* mono-nucleosomes (NCPs) were reconstituted by the standard salt-
1498 dialysis method by mixing histone octamers (or H3/H4 tetramers and H2A/H2B dimers) with
1499 '601' DNA in high salt buffer (25 mM Tris-HCl pH 7.5, 2M NaCl, 0.1 mM EDTA, 1 mM DTT) in a
1500 slide-a-lyzer mini dialysis unit (0.1 mL, ThermoFisher)(Dyer et al., 2003). Low-salt buffer (25 mM
1501 Tris-HCl pH 7.5, 0.1 mM EDTA, 1 mM DTT) was pumped in over ~24 hours in a cold room with
1502 stirring. A final dialysis was performed into NCP storage buffer (25 mM HEPES-NaOH, 10 mM
1503 NaCl, 0.1 mM EDTA, 1 mM DTT). Fluorophore-labelled nucleosomes were further purified by
1504 SEC using a 24 mL Superdex 200 increase 10/300 column equilibrated in NCP storage buffer or
1505 by extensive buffer exchange in a concentrator to remove excess fluorophore. For tri-NCPs, salt
1506 dialysis was performed as described for mono-NCPs using ~1.4x octamer to '601' sites in the
1507 presence of 0.2 equivalents of MMTV competitor DNA. Following dialysis into TEK10 (10 mM
1508 Tris-HCl pH 7.5, 0.1 mM EDTA, 10 mM KCl), trimers were precipitated by adding 4 mM $MgCl_2$,
1509 incubating on ice for 10 minutes and pelleted by centrifugation at 17,000 x g at 4 °C. The
1510 supernatant was discarded, and the pellet was gently resuspended in TEK10, and dialyzed
1511 overnight into NCP storage buffer. Tri-NCP assembly was verified by EcoRI digestion of sites
1512 located between nucleosome units.
1513
1514 For di-NCP assembly, mono-NCPs with DraIII sticky ends were assembled as described above.
1515 The strategy to make asymmetric di-NCPs was based on previously described methods(Dao et
1516 al., 2020; Poepsel et al., 2018). 100 nM of each NCP was mixed in T4 ligase buffer (50 mM

1517 Tris-HCl pH 7.5, 10 mM $MgCl_2$, 1 mM ATP, 10 mM DTT) on ice. T4 ligase (NEB) was added to a
1518 final concentration of 20 U/μL, the reaction was incubated for 30 minutes at 16 °C, and dialyzed
1519 into TEK10 for 4 hours at 4 °C. Following dialysis, $MgCl_2$ was added to a final concentration of
1520 18 mM, incubated at room temperature for 15 minutes, and pelleted at 17,000 x g at 4 °C. The
1521 pellet containing di-NCPs was resuspended in 50 μL of TEK10 and dialyzed overnight into NCP
1522 storage buffer. All chromatin substrates were analyzed for quality on 5% polyacrylamide 0.5x
1523 TBE gels monitoring fluorescence and/or DNA-staining, ensuring minimal free DNA or
1524 contaminating species. Chromatin substrates were stored on ice for no longer than one month.
1525
1526 *Design and assembly of DNA competitor fragments:* single-stranded, double-stranded, bubble,
1527 frayed, and single-stranded overhang DNA fragments were assembled by annealing ssDNA
1528 oligos (IDT) in IDT duplex buffer (30 mM HEPES-NaOH pH 7.5, 100 mM potassium acetate).
1529 Oligo mixtures were heated to 95 °C and slowly cooled to 25 °C stepwise over 1 hour in a
1530 thermocycler. For NMR experiments, dsDNA and bubble-DNA were buffer exchanged into NMR
1531 buffer in a spin concentrator (Amicon). The sequences of oligos used are as follows. For
1532 ssDNA, dsDNA, bubbleDNA, and ssOverhang a common “bottom” oligo was used
1533 (ggtacacaattgcgctggtaccccaggcgtcgtagg). The oligos annealed to the “bottom” oligo were as
1534 follows: (dsDNA-top: cctacgacgcctggggtaccagcgcaattgtgtacc; bubbleDNA-top:
1535 cctacgacgcctggctctttcccgcaattgtgtacc; ssOverhang-top: ccgcaattgtgtac). For the frayed DNA,
1536 the annealed oligos were as follows: (frayedDNA-top: ggtacacaattgcgccaggcgtcgtaggctggtacc;
1537 frayedDNA-bottom: ctctttcccctacgacgcctggcgcaattgtgtacc).
1538
1539 **Nucleosome ubiquitylation assays**
1540 *Time-course H2A-Ub assays:* The general setup for time-course H2A-Ub assays was a reaction
1541 mixture containing 0.2 μM E1 (UBA1), 1 μM E2 (UBE2D3), 30 μM ubiquitin, 0.5 μM NCP

1542 substrate, and 12.5-100 nM E3 (depending on the assay), assembled in 30 μL of reaction buffer
1543 (25 mM HEPES-NaOH pH 7.5, 150 mM NaCl). For assays containing di-NCPs, 10 nM of
1544 fluorophore-labelled di-NCP substrate was mixed with 0.5 μM unlabeled NCP^{147} substrate in the
1545 same reaction tube to facilitate quantifiable reaction kinetics. Critically, the salt concentration of
1546 each reaction within an assay was rigorously controlled, as H2A-Ub kinetics are extremely
1547 sensitive to differences in buffer ionic strength. 5 μL of each reaction was mixed 1:1 with 2x
1548 SDS-PAGE load dye as a zero time-point. The mixtures were brought to 37 °C in a heat block,
1549 and 1 μL of 100 mM $MgCl_2$/ATP was added (4 mM final concentration) to initiate the reaction,
1550 and the indicated time-points were obtained by diluting 5 μL the reaction 1:1 with 2x SDS-PAGE
1551 load dye. For experiments with tri-NCPs, the concentration of nucleosome units in the reaction
1552 was normalized to NCP^{147} and NCP^{185} (0.5 μM NCP unit or 0.17 μM tri-NCP), and reactions
1553 were initiated with 2 mM ATP and 1 mM $MgCl_2$.
1554
1555 Gel samples were run on 15% SDS-PAGE gels and visualized by in-gel fluorescence monitoring
1556 a fluorophore conjugated to the N-terminus of H2A. Alternatively, some assays were visualized
1557 by Western blot for H2A (EMD Millipore, 07-146) or a VSVG epitope tag on the N-terminal tag of
1558 H2A (Sigma, V4888) and a fluorescently labelled secondary antibody (Cell Signaling, 5151S).
1559 Gels and blots were imaged on a Li-Cor Odyssey imager (Li-Cor). Band quantification was
1560 performed using Image Studio software (Li-Cor) by drawing a box encompassing the unmodified
1561 H2A band to measure its intensity, performing background subtraction, and normalizing to the
1562 zero time-point of a given reaction.
1563
1564 *Inhibition of H2A-Ub by competitor DNA:* A reaction mixture containing 0.2 μM E1 (UBA1), 3 μM
1565 E2 (UBE2D3), 30 μM ubiquitin, 0.5 μM NCP substrate, and 50 nM E3 (or 750 nM for
1566 $BRCA1^{RING}$/$BARD1^{RING}$) was assembled in 9 μL of reaction buffer (25 mM HEPES-NaOH pH
1567 7.5, 100 mM NaCl) in PCR strips. To that, 1 μL of DNA competitor at 10x concentration was

1568 added. Reactions were brought to 37 °C in a thermocycler, started by addition of 5 µL of 10 mM
1569 ATP/$MgCl_2$ in reaction buffer, and allowed to proceed for 12-20 minutes depending on the E3.
1570 Reactions were stopped by addition of 10 µL of 4x fluorescence sample load dye (Li-Cor),
1571 resolved on a 15% SDS-PAGE gel, and visualized using a Li-Cor Odyssey imager.
1572 Quantification was performed as described above, monitoring the intensity of unmodified H2A,
1573 and normalizing each reaction to a -ATP reaction.
1574
1575 *Auto-ubiquitylation assay:* Reactions were assembled with 0.2 µM E1 (UBA1), 1 µM E2
1576 (UBE2D3), 10 µM ubiquitin (Q2C-Alexa Fluor 680), and 0.2 µM of the indicated E3 in buffer (25
1577 mM HEPES-NaOH pH 7.5, 50 mM NaCl), and were initiated by addition of 5 mM ATP/$MgCl_2$.
1578 After 60 minutes at 37 °C, reactions were quenched by mixing 1:1 with 4x fluorescence sample
1579 load dye (Li-Cor), resolved on a 4-20% SDS-PAGE gel (BioRad), and visualized using a Li-Cor
1580 Odyssey imager.
1581
1582 **Nucleosome binding assays**
1583 *Electrophoretic mobility shift assay:* For EMSA experiments, 5 µL of 10 nM of substrate (NCPs
1584 with either H2A G-1C labelled with Alexa Fluor 680 or DNA/NCPs labelled with IRDye700) were
1585 mixed with 5 µL of indicated RING/RING heterodimer or BARD1 IDR constructs (2x
1586 concentrated) in EMSA buffer (15 mM Tris-HCl pH 7.5, 90 mM NaCl, 1 mM DTT, 0.1 mg/mL
1587 BSA, 0.05% triton X-100) in PCR strips. Binding was allowed to proceed for 10 minutes at room
1588 temperature, followed by 5 minutes on ice. 5 µL of 25% sucrose was added to each tube, and
1589 15 µL of sample was loaded onto 5% polyacrylamide native gels (0.5x TBE) in pre-chilled 0.5x
1590 TBE buffer. Gels were run at 4 °C for 90-120 minutes at 110V and visualized using a Li-Cor
1591 Odessey scanner (Li-Cor).
1592

1593 *Fluorescence-quenching binding experiments:* Assay set up was performed essentially as
1594 previously described(Hu et al., 2021). 10 µL of 10 nM NCPs with Oregon green 488 conjugated
1595 to H2B D51C in low-salt fluorescence buffer (25 mM Tris-HCl pH 7.5, 10 mM NaCl, 0.01%
1596 CHAPS, 0.01% NP40, 0.1 mg/ml BSA, 1 mM DTT) were mixed with the 10 µL of the indicated
1597 BRCA1/BARD1 construct at 2x concentration in high-salt fluorescence buffer containing either
1598 90 mM, 190 mM, or 290 mM NaCl, depending on the assay, in a 384-well low volume black
1599 round bottom polystyrene non-binding surface microplate (Corning). Plates were briefly mixed,
1600 incubated at 22 °C for 10-15 minutes, and scanned using a BioTek Synergy Neo2 plate reader
1601 equipped with a fluorescence filter (excitation: 485/20 nm, emission: 528/20 nm). The gain was
1602 set to 100 for all experiments. Two to three technical replicates for each independent replicate
1603 experiment (fresh NCP and BRCA1/BARD1 dilutions) were performed, and the readings from
1604 two scans were averaged. BRCA1/BARD1/nucleosome binding interactions were quantitatively
1605 analyzed by fluorescence quenching assuming the following systems of equations:

1606 $$\theta = \frac{K_D + [NCP] + [BCBD] - \sqrt{(K_D + [NCP] + [BCBD])^2 - 4 \times [NCP] \times [BCBD]}}{2 \times [NCP]}$$

1607 $$F = [NCP] \times F_{NCP} \times (1 - q_{BCBD} \times \theta) + N(0, error)$$

1608 where θ is the fraction of nucleosome bound by BRCA1/BARD1 (BCBD), F_{NCP} is the
1609 fluorescence per nucleosome, q_{BCBD} is the fraction of fluorescence quenching per
1610 BRCA1/BARD1 binding, and fluorescence measurements are gaussian distributed with mean 0.
1611 Maximum likelihood parameter estimates were determined using custom Python scripts with
1612 optimization by a differential evolution algorithm implemented in Scipy(Virtanen et al., 2020). K_d
1613 and q_{BCBD} were separately estimated for each BRCA1/BARD1 construct, and NCP
1614 concentration was treated as a random effect per individual dilutions from higher concentration
1615 stock solutions, with the total number of model parameters being equal to number of NCP
1616 dilutions + (2 x number of BCBD constructs) + 2. The 95% confidence limits were estimated by
1617 computing the profile likelihood with an applied Bonferroni correction.

1618

1619 **UV-induced Bpa crosslinking**

1620 NCPs and DNA for UV-induced crosslinking assays were reconstituted using a 185-bp '601'
1621 sequence labeled with an IRdye700 fluorophore (described above). 50 nM NCPs or DNA were
1622 incubated with 500 nM of the BRCA1$^{1-104}$-$(GS)_6$-BARD1$^{26-221}$ fusion (wild-type or with different
1623 Bpa-incorporated sites L120Bpa, W146Bpa, Y180Bpa, A195Bpa, W218Bpa) for 15 minutes at
1624 4°C in 30 uL UV Crosslinking buffer (20 mM HEPES-NaOH pH 7.5, 100 mM NaCl) in a 96-well
1625 clear round bottom polystyrene non-treated microplate (Corning). Following incubation, 5 µL
1626 was added to 5 µL 2X SDS-PAGE gel-loading dye for the -UV sample. Samples were then
1627 subjected to UV irradiation (365 nm) using a Blak-Ray B-100AP/R High Intensity UV Lamp
1628 (UVP) from 20 cm for 30 minutes at 4°C. Following irradiation, 5 µL was added to 5 µL of 2x
1629 SDS-PAGE gel-loading dye. Samples were heated at 60°C for 5 minutes and separated on 10%
1630 SDS-PAGE gels. Gels were visualized using a Li-Cor Odyssey scanner (Li-Cor). Band
1631 quantification was performed using Image Studio software (Li-Cor) by drawing a box measuring
1632 the total band intensity for each crosslinked product, subtracting the background signal, and
1633 normalizing to the crosslinked band of the L120Bpa fusion mutant. For the Bpa UV crosslinking
1634 DNA competition assays, 50 nM NCPs were incubated with 500 nM BRCA1-f-BARD1^{221}
1635 (W146Bpa or A195Bpa) with varying amounts of competitor 36-mer dsDNA or bubble-DNA (0,
1636 0.3125, 0.625, 1.25, 2.5, 5, or 10 μM) for 15 minutes at 4°C, and assays were performed as
1637 described above.

1638

1639 **Chemical Crosslinking and Mass Spectrometry Analysis**

1640 *Sample preparation:* Reactions were 90 µL of protein/nucleosome mix containing 2 mM
1641 BRCA1^{RING}/BARD1^{FL} and 2 mM of unmodified H2A or H2A K15-Ub nucleosomes wrapped with
1642 147-bp '601' DNA in crosslinking bufffer (25 mM HEPES-NaOH pH 7.5, 150 mM NaCl, 1%
1643 glycerol, 1 mM DTT) plus 3.06 µL of 14.5 mM DSS or BS3 (final concentration 0.5 mM) (DSS:

1644 disuccinimidyl suberate, BS3: bis(sulfosuccinimidyl)suberate, ThermoFisher). Crosslinking was
1645 carried out for 10, 30 or 45 mins at room temperature before removing 30 µL and quenching by
1646 addition of 3 µL of 1 M ammonium bicarbonate at room temperature for 30 minutes. Four
1647 separate reaction conditions were performed: (1) WT-NCP DSS; (2) WT-NCP BS3; (3) K15Ub-
1648 NCP DSS; (4) K15Ub-NCP BS3. After quenching, 9 µL of each sample at each timepoint was
1649 analyzed by SDS-PAGE **(see Extended Data Fig 10a)** and the remainder was stored at -80°C
1650 until processing for mass spectrometry analysis.
1651
1652 Reactions were prepared for MS analysis by bringing them up to 0.1% PPS silent surfactant
1653 (Expedion Inc.), 5 mM TCEP. Samples were reduced for 60 mins at 60°C in an Eppendorf
1654 Thermomixer with shaking (1200 rpm). Alkylation was performed at room temperature in the
1655 dark for 30 mins with 6 mM iodoacetamide. Excess iodoacetamide was quenched by addition of
1656 5 mM DTT and samples were then digested by trypsin digestion (Sequencing Grade Modified
1657 Trypsin, Promega Corp) at 37°C for 6 hours in a Thermomixer with shaking (1000 rpm) at a
1658 substrate to enzyme ratio of 15:1 prior to acidification with 250 mM HCl (final concentration).
1659 Acidified samples were incubated for 1 hour at room temperature, spun at max speed in a
1660 microfuge and supernatants containing peptides were transferred to autosampler vials and
1661 stored at -80°C until analysis.
1662
1663 *Chromatography:* Mass spectrometry and data analysis was based on previously described
1664 methods(Zelter et al., 2015). For each injection, 3 µl of protein digests were loaded by
1665 autosampler onto a 150-µm Kasil fritted trap packed with 2 cm of Reprosil-Pur C18-AQ (3-µm
1666 bead diameter, Dr. Maisch) at a flow rate of 2.5 µl/min. After desalting with 8 µl of 0.1% formic
1667 acid plus 2% acetonitrile, the trap was brought online with a Self-Packed PicoFrit Column (New
1668 Objective part number PF360-75-10-N-5, 75 µm i.d.) packed with 30 cm of Reprosil-Pur
1669 C18-AQ (3-µm bead diameter, Dr. Maisch) mounted to a heated nanospray ionization source

1670 (CorSolutions LLC) set at 50°C and placed in line with a Thermo Scientific EASY-nLC 1200
1671 UPLC pump plus autosampler.
1672
1673 Peptides were eluted from the column at 0.25 µL/min using an acetonitrile gradient consisting of
1674 the following steps: (1) 0-10 mins; 6-10% B; (2) 10-90 mins; 10-32% B; (3) 100-130 mins; 32-
1675 75% B; (4) 130-135 mins; 75% B; (5) 135-136 mins; 75-100% B; (6) 136-151 mins; 100% B,
1676 followed by re-equilibration to 0% buffer B prior to the subsequent injection. Buffer A was: 0.1%
1677 formic acid in water and buffer B was 0.1% formic acid 80% acetonitrile.
1678
1679 *Data acquisition:* A Thermo Fisher Scientific Exploris 480 was used to perform mass
1680 spectrometry in positive ion mode with the following settings. Data dependent acquisition (DDA)
1681 mode was used with a maximum of 20 tandem MS (MS/MS) spectra acquired per MS spectrum
1682 (scan range of *m/z* 400–1,600). The resolution for MS and MS/MS was 60,000 at *m/z* 200. The
1683 normalized automatic gain control targets for both MS and MS/MS were set to 100%, and the
1684 maximum injection times were 50 and 100 ms for MS and MS/MS scans, respectively. MS/MS
1685 spectra were acquired using an isolation width of 2 *m/z* and a normalized collision energy of 27.
1686 MS/MS acquisitions were prevented for +1, +2, ≥+6 or undefined precursor charge states.
1687 Dynamic exclusion was set for 10 seconds. MS and MS/MS spectra were collected in centroid
1688 mode.
1689
1690 *MS data processing – identification of crosslinked peptides:* Raw mass spectra were converted
1691 into mzML using ProteoWizard's msconvert(Chambers et al., 2012). All proteins in the sample
1692 were identified using Comet(Eng et al., 2013) searching against a database including the entire
1693 *S. frugiperda*, *E. coli* and *H. sapiens* proteomes (Uniprot 7108, 83333 and 9606, respectively)
1694 plus common contaminants (https://www.thegpm.org/crap/) along with the sequences of all
1695 heterologously expressed proteins (FLAG-BRCA1, P38398; TwinStrepII-BARD1, Q99728; H2A-

1696 2A, Q99728; H2B-1K, O60814 ; H3.2 (C110A), Q71DI3; H4, P62805; Ub G76C, sequence
1697 derived from P0CG48). Smaller search databases were made for subsequent XL searching
1698 consisting only of proteins identified in initial comet searches by at least 3 peptides with a
1699 Percolator assigned q-value of ≤ 0.01. Decoy databases consisted of the corresponding set of
1700 reversed protein sequences. Cross-linked peptides were identified within these proteins by
1701 Kojak version 2.0.0-alpha8 available at (http://www.kojak-ms.org/)(Hoopmann et al., 2015). A
1702 statistically meaningful q-value was assigned to each peptide spectrum match (PSM) through
1703 analysis of the target and decoy PSM distributions using Percolator version 2.08(Käll et al.,
1704 2007). All data reported in this paper were filtered to show hits to the target proteins that had a
1705 Percolator assigned peptide level q value ≤ 0.05.
1706
1707 **NMR experiments and resonance assignments.**
1708 All spectra were collected at 25° C in NMR buffer (25 mM MOPS-NaOH, 100 mM NaCl, 1 mM
1709 EDTA, and 0.5 mM TCEP, pH 7.0) with 7% D_2O. NMR HSQC and titration data were completed
1710 on a Bruker 800 MHz Avance III spectrometer with cyroprobe. (^{1}H,^{15}N)-HSQC spectra were
1711 collected on the following ^{15}N-BARD1 IDR constructs: BARD1 Ser-124-424, Ser-124-270, 269-
1712 424, and Ser-141-216.
1713
1714 (^{1}H,^{15}N)- and (^{1}H,^{13}C)-HSQC titration experiments were completed for BARD1 IDR + 36mer-
1715 dsDNA or 36mer-bubDNA by adding unlabeled DNA to 150 μM [^{13}C,^{15}N]-BARD1 124-270 or
1716 150 μM [^{13}C,^{15}N]-BARD1 Ser-141-216, maintaining a constant concentration of the labeled
1717 species. Only apo and 1:1 spectra for the [^{13}C,^{15}N] BARD1 Ser-141-216 construct were
1718 obtained since intermediate titration points resulted in loss of sample. Additionally, titration
1719 spectra with nucleosome were collected for 150 μM [^{13}C,^{15}N]-BARD1 124-270 + 0.05x NCP^{147}.
1720 A (^{1}H,^{15}N)-HSQC was collected on 150 μM ^{15}N-BARD1 269-424 + 150 μM 28mer-dsDNA.
1721

1722 Dynamics experiments were collected on a Bruker 500 MHz Avance III spectrometer with a
1723 room temperature probe. T_1 and T_2 ^{15}N-Trosy HSQC experiments for 150 μM [^{13}C,^{15}N]-BARD1
1724 Ser-141-216, 150 μM [^{13}C,^{15}N]-BARD1 Ser-141-216 + 150 μM 36mer-dsDNA, and 150 μM
1725 [^{13}C,^{15}N]-BARD1 Ser-141-216 + 150 μM 36mer-bubble-DNA were collected in an interleaved
1726 manner with 8 points each(G. Zhu et al., 2000). T_1 delays were 10, 40, 80, 120, 160, 320, 640,
1727 and 1000 ms; T_2 cpmg loop delays were 8.48, 16.96, 25.44, 25.44, 42.40, 50.88, 67.84, and
1728 84.80 ms. T_1 and T_2 for each residue were fitted to a single exponential with errors reflecting the
1729 quality in the fit. Residues corresponding to peaks with overlapping intensities were excluded
1730 from the analysis.
1731
1732 Backbone chemical shift assignments were determined from standard backbone triple-
1733 resonance experiments (HNCA, HNCOCA, HNCOCACB, HNCACB, HNCO, and HNCACO) and
1734 an HNHA experiment using a Bruker 800 MHz Avance III spectrometer with cryoprobe. The 3D
1735 data were collected for 500 μM [^{13}C,^{15}N]-BARD1 Ser-124-270 and 500 μM [^{13}C,^{15}N]-BARD1
1736 Ser-141-216. Assignments from the shorter construct were transferred as appropriate to the
1737 longer BARD1 construct. HNCACB and HNCOCACB spectra were collected on the 1:1 samples
1738 of 150 μM [^{13}C,^{15}N]-BARD1 Ser-141-216 with either 36mer dsDNA or 36mer bubble-DNA.
1739
1740 The NH chemical shift perturbation was calculated according to $\Delta\delta_{NH}$ (ppm) = sqrt [$\Delta\delta_H^2$ +
1741 $(\Delta\delta_N/5)^2$]. Component ^{1}H and ^{15}N chemical shift differences are (free – bound) in ppm. The
1742 CaCb CSP was calculated according to $\Delta\delta_{CaCb}$ (ppm) = 0.25*[$(C\alpha\text{-}C\beta)_{free}$-$(C\alpha\text{-}C\beta)_{bound}$].
1743 Secondary structure propensity (SSP) was determined from $\Delta\delta(C\alpha\text{-}C\beta) = (C\alpha\text{-}C\beta)_{measured} - (C\alpha\text{-}$
1744 $C\beta)_{random\ coil}$, where the random coil shifts were generated from BARD1 IDR sequence using a
1745 webserver (https://spin.niddk.nih.gov/bax/nmrserver/Poulsen_rc_CS/)(Kjaergaard & Poulsen,
1746 2011).
1747

1748 **Multiple Sequence Alignment**

1749 Mammalian BARD1 ortholog sequences were downloaded from Ensembl (v106), globally
1750 aligned using MAFFT(Katoh & Standley, 2013), and trimmed to BARD1 residues 124-270.

1751

1752 **Materials, Data, and Code availability Statement**

1753 Source data for H2A-Ub and binding assays as well as uncropped gels and blots are included
1754 as supplemental files. For crosslinking mass-spectrometry analysis, the complete unfiltered list
1755 of all PSMs and their Percolator assigned q values are available on the ProXL web
1756 application(Riffle et al., 2016, 2019) https://proxl.yeastrc.org/proxl/p/bard1nucleosome along
1757 with the raw MS spectra and search parameters used. In addition, complete search algorithm
1758 configuration files, fasta search databases, raw search output and raw MS data files were
1759 deposited to the ProteomeXchange Consortium via the PRIDE(Vizcaíno et al., 2009) partner
1760 repository with the dataset identifier PXD035345. NMR chemical shift assignments for BARD1
1761 Ser-141-216 and associated DNA-bound assignments have been deposited to the Biological
1762 Magnetic Resonance Bank with dataset identifiers 51523 (apo), 51524 (with dsDNA), 51525
1763 (with bubble-DNA). Python scripts used to analyze and plot fluorescence-based binding data
1764 are included with this manuscript. Plasmid reagents generated in this study can be obtained
1765 upon request from the corresponding author Dr. Rachel Klevit.